Synthesis and Characterization of Inorganic Nanorods and Nanotubes

and

Kirkendall effect-induced Transformations of Metal Nanowires to Oxide or Chalcogenide Nanotubes

A Thesis

submitted in partial fulfilment of the requirements of the degree of Master of Science [Engg.]

By

Kalyan Raidongia

Chemistry and Physics of Materials Unit

Jawaharalal Nehru Centre for Advanced Scientific Research

(A Deemed University)
Bangalore – 560 064
April 2007

Dedicated

To

My Parents

DECLARATION

I hereby declare that the matter embodied in this thesis entitled **"Synthesis and characterization of inorganic nanorods and nanotubes and Kirkendall effect-induced transformations of metal nanowires to oxides or chalcogenide nanotubes"** is the result of investigations carried out by me under the supervision of Prof. C. N. Rao and Dr. M. Eswaramoorthy, at the Chemistry and Physics of Materials Unit, Jawaharlal Nehru Centre for Advanced Scientific Research, Bangalore, India and that it has not been submitted elsewhere for the award of any degree or diploma.

In keeping with the general practice in reporting scientific observations, due acknowledgement has been made whenever the work described is based on the findings of other investigators.

Kalyan Raidongia

Kalyan Raidongia

CERTIFICATE

We hereby certify that the matter embodied in this thesis entitled "**Synthesis and characterization of inorganic nanorods and nanotubes and Kirkendall effect-induced transformations of metal nanowires to oxides or chalcogenide nanotubes**" has been carried out by Mr. Kalyan Raidongia at the Chemistry and Physics of Materials Unit, Jawaharlal Nehru Centre for Advanced Scientific Research, Bangalore, India under our supervision and that it has not been submitted elsewhere for the award of any degree or diploma.

Prof. C. N. R. Rao, FRS

(Research Supervisor)

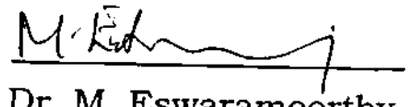

Dr. M. Eswaramoorthy

(Research Supervisor)

Contents

Acknowledgements

I express my sincere gratitude to Prof. C. N. R. Rao, FRS for suggesting me research problems and guiding me throughout. He has been a constant source of inspiration for me. It has been a wonderful experience working with him. I am thankful to him for giving me an opportunity to work under his guidance.

I wish to express my sincere gratitude to Dr. M. Eswaramoorthy for the kind encouraging guidance he gave me all through the course of these investigations. I am particularly grateful to him for the discussions I had with him. He has been a constant source of inspiration to me. I am thankful to him for giving me an opportunity to work under his guidance.

I am thankful to the faculty members of JNC and IISc for the courses that have been extremely beneficial to this study. In particular, I would like to thank Dr. A. Sundaresan, Dr. M. Eswaramoorthy, Prof. U. V Waghmare. Prof. Chandrabhas Narayana, Prof. Swapan K Pati, and Prof. S. Balasubramanian from JNC and Prof. S. Ranganathan from IISc.

I am thankful to Basavaraj, Usha Madam, Anil, Vasu and Selvi for their help with the various characterization techniques.

I would like to thank my lab members Dinesh, Saikrishna and KKR Datta for their constant help and co-operation.

I would like to express my sincere thanks to Dr. A. Govindaraj and Vivek who have helped me a great deal in carrying out some experiments.

I am thankful to INI center and Convenor of the center Prof. K. Chattopadhyay, IISC for TEM facility.

I would like to thank Mrs. Rao for her encouraging words and hospitality.

I am thankful to all academic staff members (Mrs. Sukanya, Dr. Princy).

I am thankful to office members (Mrs. Sashi, Gowda, Victor and Mrs. Sudha).

Thanks to Prof. U. V. Waghmare, Prof. Swapan. K. Pati and Dr. Mousumi Upadhyay-Kahaly for carrying out first-principles density functional theory based calculations to understand the structure and properties of BC_4N nanotubes.

Special thanks to my friends Madhu, Venky, Pranab, Rak, Nivas, Gomathi, subrahmanyam, Pavan, Bhuvana, Gopal, Srini, Reji, Thiru, Vijay, Ved, Sahu, Rout, Sairam, Suidapta, Leela, Anil, Claudy, Guru, Sameer, Raj, Bhat, Shipra, Neenu, Kalyani, Kanishka, Prakash, Sudip, Nasir, Ramkirshna, Sandeep and Basanth

A special note of thanks to friends in IISc Gitish, Mahanta, Abhijit, and Shymol for helping me in literature search.

I wish to express my gratitude to my parents, brother, beloved, her parents, Tatuman and Malini for their unconditional support.

Preface

Nanomaterials research is one of the most dynamic and fastest growing areas in the fields of science, engineering and medicine. These materials exhibit unique properties compared to their counterpart bulk materials. A great deal of efforts is being devoted on the synthesis and properties of these materials in order to understand and use them.

Chapter 1 gives a brief overview of nanomaterials.

Chapter 2 deals with the synthesis and characterization of metal oxides nanorod brushes. Nanorod brushes or Al_2O_3, MoO_3 and ZnO have been synthesised using amorpous carbon nanotubes brushes as the starting materials.

In chapter 3, synthesis, characterization and properties of homogeneous BC_4N nanotube brushes has been discussed. The nanotubes which are stable up to 900 °C can exhibit a selective uptake of CO_2. The insulating and nonmagnetic nanotubes can stabilize nanoparticles on its surface.

Chapter 4 deals with the transformations of elemental nanowires of metals and silicon to the nanotubes of corresponding oxides and chalcogenides through Kirkendall effect. Special attention has been paid to the mechanism and the kinetics of the nanowire to nanotube transformation.

CHAPTER 1

A Brief Overview of Nanomaterials

1.1. Introduction

Materials with structural features between those of single atoms or molecules and bulk materials are known as nanomaterials. The prefix "nano," denoting a factor of 10^{-9} has derived from the Greek "nanos," meaning "dwarf". Nanomaterials have at least one dimension in the nanometer (*i.e.* a billionth of a meter) range. Properties of these materials are significantly different from those of atoms as well as bulk materials. Similar to quantum mechanics, on nanometer length scale, materials may possess new physical properties or exhibit new physical phenomena. Some of these properties are already known. For example, band gaps of semiconductors can be tuned by varying their size and shape.[1] There may be many more unique physical properties not known to us yet. These new physical properties or phenomena will not only satisfy everlasting human curiosity, but also promise new advancement in technology. For example, ultra-strong, ultra-light, multifunctional materials are possible from hierarchical nanostructures.

Nanomaterials also promise the possibility of the miniaturization of current and new instruments, sensors and machines that will greatly impact the world we live in.

Unwittingly, nanomaterials have been fascinating human minds over thousands of years. Brilliant red colour of gold nanoparticles was used by the Chinese in colouring their ceramic porcelains more than a thousand years ago. Throughout Europe metal nanoparticles have been using in stained glass windows of cathedrals since 17th century. Although nanomaterials had been used thousand years ago the first systematic study on these materials was carried out in the 1850s by Michael Faraday. In those groundbreaking studies he has observed the particles size dependent colour of the gold sols. The tremendous potentials and the importance of nanotechnology were realized by Nobel laureate Richard Feynman. He has motivated the researchers towards the field of nanoscience in his often-cited lecture entitled "There is plenty of room at the bottom" delivered at the annual meeting of the American Physical Society at the California Institute of Technology (Caltech) in 1959. The explosive growth of the nanotechnology research started in 1981 when Binnig and Rohrer at IBM Zurich invented the scanning tunneling microscope (STM), the first instrument to generate real space images of surfaces with atomic resolution.[3] This discovery was recognized by the 1986 Nobel Prize in Physics, along with the inventor of the electron microscope.

In recent years, nanotechnology has become one of the most important and exciting forefront research areas in chemistry, physics, engineering and biology. This is primarily because of the availability of new synthetic strategies and tools for characterization and manipulation of the nanomaterials. Scanning tunneling microscope (STM) image of the quantum corral of 48 Fe atoms placed in a circle of 7.5 nm radius shows the current status of characterization tools for nanomaterials (Figure 1). Heinrich and his co-workers were able to probe magnetic anisotropy in individual

Figure 1. STM image of a quantum corral of 48 Fe atoms placed in a circle of 7.3 nm [IBM Research].

atoms, opening up the possibility of giant magnetic anisotropy that can be engineered at the atomic scale.[4] A large number of innovative and elegant synthetic strategies have been developed to synthesize nanomaterials of almost all chemical compositions with a wide variety of morphology and size. Based on the number of dimension present in their shape nanomaterials can be classified into three

broad categories: zero dimensional (0D), one dimensional (1D) and two dimensional (2D).

In nanomaterials, the electronic energy levels are not continuous, as in the case of bulk but are discrete due to the confinement of the electron wave-function to the physical dimensions of the particles.[5] A schematic illustration of the density of states in one band of a semiconductor as a function of dimensions is shown in Figure 2. The density of states changes remarkably with dimension. In case of 3D it is a continuous function while for 2D nanostructures it is a step function with steps occurring at the energy of each quantized level. In the case of 1D nanostructures, van Hove singularities are observed and for 0D nanostructures, the density of states shows quantization at particular energy levels.

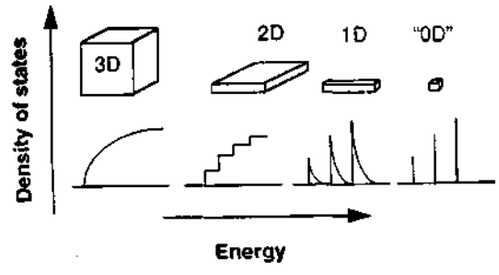

Figure 2. Density of states in one band of a semiconductor as a function of dimensions

1. 2. Zero-dimensional nanomaterials

Zero dimensional (0D) nanomaterials have all the three dimensions in the nanometer regime (1-100 nm). These materials are usually denoted by nanoparticles, nanoclusters, nanocrystals or

quantum dots. The term nanoparticles generally encompass all the zero dimensional nanomaterials. Nanoclusters refer to a tiny chunk of the bulk measuring (1-10 nm) with well defined arrangement of a definite number of constituent atoms. The atoms arrange themselves on the basis of maximizing the number of bonds and minimizing the number of atoms on the surface. They nucleate from atoms and enter into a size range where they behave electronically as molecular nanoclusters. As the number of atoms increases further they cross over into nanocrystals where the quantum size effects dominate their electronic properties. Nanocrystals usually referred to single-crystalline 0D nanomaterials. A special case of nanocrystals that are comprised of semiconductors is known as a quantum dot.[6] Figure 3 shows the TEM images of CdSe and CdS/HgS/CdS quantum dots prepared by Weller and co-workers.[7]

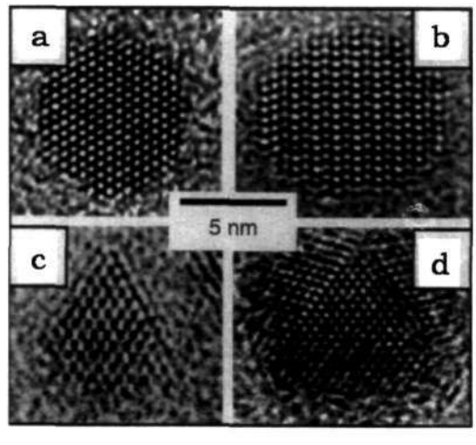

Figure 3. (a and b) TEM images of CdSe nanocrystals with hexagonal structure, (c and d) TEM image of CdS/HgS/CdS quantum dot quantum well.

Zero dimensional nanomaterials are currently an area of intense scientific research, due to their fascinating properties and a variety of potential applications. The properties of nanocrystals are different from the corresponding bulk materials and depend on the size.[8] A conducting material could be transformed to an insulator by reducing its size to nanometer regime.[8] Similarly, a nanocrystal of a ferromagnetic material can be paramagnetic in nature. Copper nanoparticles smaller than 50 nm are considered super hard materials that do not exhibit the same malleability and ductility as bulk copper. Cadmium selenide can be made to yield any colour in the spectrum simply by controlling their particle size in nanometer regime.[9]

The electronic absorption of the metal nanocrystals is dominated by surface plasmons, the collective oscillations of the free electron gas. Light of definite energy can excite the surface plasmons which is characteristic of the size of metal nanocrystals. Surface plasmons also impart characteristic colours to the metal sols. The dependence of surface plasmons excitation energy on the dielectric constant of the surrounding medium and the diameter of the nanocrystal was established by Mie and others, well-known as "Mie theory".[10-13] In contrast to metals nanoparticles, in semiconductor nanocrystals the absorption is dominated by exciton. The absorption band that originated from the three dimensional confinement of the excitons, can be systematically varied by changing the size of the

semiconductor nanocrystals.[14-16] The size quantization effects in semiconductor nanocrystals are described by Brus based on the effective mass approximation.[17,18] In addition to interesting absorption properties, the semiconductor nanocrystals also exhibit luminescent behaviour.[19-22] The emission of these nanocrystals can be tuned by varying the diameter or diameter distribution of the nanocrystals.

Synthesis forms an essential component of nanoscience and nanotechnology. Various physical and chemical methods have been demonstrated to generate 0D nanomaterials.

Physical methods

Physical methods are usually employed for the large scale production of nanoparticles with high purity. However, the physical methods have poor control over the shape and size distributions. Most commonly used physical methods are metal evaporation, ball milling, and electrodeposition. Metal evaporation is done by various techniques like, arc discharge, ion sputtering, laser ablation, laser pyrolysis and spray pyrolysis.[23] All these methods involve the evaporation of a solid material to form a supersaturated vapor followed by nucleation of the nanoparticles. The size of the nanoparticles can be controlled either by choosing a proper source of evaporation, or by slowing the growth rate by introducing gas molecules to collide with the particles.

Chemical methods

Several chemical methods have been developed to achieve a good control over size, shape and composition of the nanoparticles. Commonly encountered chemical methods are the reduction of metal salts, thermal decomposition of organometallic compounds and sol-gel processes. Chemical evolution of a nanoparticle involves three distinct stages; seeding, particle growth and growth termination by capping. Control over these stages is essential to obtain monodisperse nanoparticles of a definite size and shape with a desired chemical composition. Chemical methods have been employed to obtain nanoparticles of wide variety of materials including metals, alloys, semi-conductors, ceramics and polymers.[24,25]

1. 3. One-dimensional nanomaterials

One-dimensional nanomaterials (1D) have one macro scopic dimension in the micrometer range and remaining two are in the nanometer regime. Nanotubes, nanowires, nanorods, nanobelts and nanohelics are well-studied example of 1D nanomaterials. A range of unique properties such as thermal, mechanical, electronic, optoelectronic, optical, nonlinear optical and field emission are associated with 1D nanomaterials. The dependence of electrical and thermal transport properties on 1D quantum confinement has been studied by using these nanomaterials. They can be also important as both interconnect and functional units in the fabrication of

electronic, optoelectronic, electrochemical and electromechanical devices with nano scale dimensions.

Most popular and widely studied 1D nanomaterials are carbon nanotubes (CNTs). The nanotubes discovered by Iijima,[26] as an electron microscopic marvel has opened up a new era in science and technology. There has been numerous research activity related to the synthesis, structure, properties and applications of CNTs. The strongest and the stiffest materials on the earth have remarkable electronic properties and many other unique characteristics. Due to their novel properties CNTs can find applications in diverse fields like materials science, medicinal chemistry and engineering. A number of techniques have been developed to produce carbon nanotubes in sizeable quantities, including arc discharge, laser ablation and chemical vapour deposition. CNTs are categorized as single-walled nanotubes (SWNTs), double-wall nanotubes (DWNTs) and multi-wall nanotubes (MWNTs), based on the number of graphene layers rolled in on themselves to form the tube shape. Figure 4 shows the TEM images of single-wall, double-wall and multi-wall CNTs. [27-29]

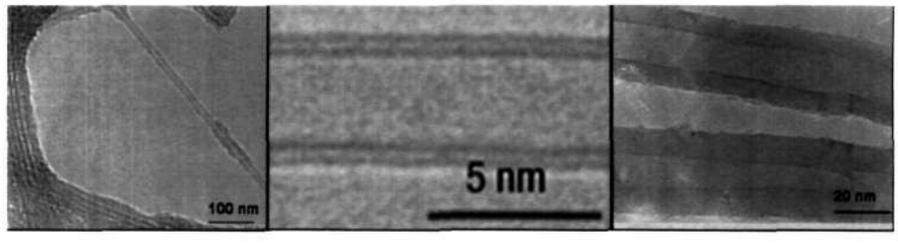

Figure 4. TEM images of (a) SWNTs, (b) DWNT, and (c) MWNTs

A large number of synthetic strategies have been adopted to fabricate 1D nanomaterials with different morphologies.[30] These synthetic strategies can be generally grouped into four categories:

(1) Spontaneous growth:

(a) Evaporation (or dissolution)-condensation

(b) Vapor (or solution)-liquid-solid (VLS or SLS) growth

(c) Stress-induced recrystallization

(2) Template-based synthesis:

(a) Electrodeposition route

(b) Direct template filling

(3) Electrospinning

(4) Lithography

Spontaneous growth

Spontaneous growth of materials is driven by the reduction of Gibbs free energy. The reduction of Gibbs free energy can be achieved by phase transformation, chemical reaction or release of stress. For the formation of a 1D nanomaterials, the crystals have to grow along a certain orientation faster than other directions. For 1D nanomaterials of uniform diameter the crystals have to grow only in one direction and growth along other directions has to restrict. The growth conditions, defects and the impurities on the growth surfaces can affect the morphology of the final products.

There are several mechanisms to result preferential growth in one direction for example

(a) Different facets in a crystal have different growth rate. For example, in silicon with a diamond structure, the growth rate of {1 1 1} facets is smaller than that of {1 1 0}.

(b) Presence of imperfections in specific crystal directions such as screw dislocation.

(c) Preferential accumulation or poisoning by impurities on specific facets.

The evaporation-condensation growth is one of the oldest and most widely used techniques for growing one dimensional nanomaterials. In 1955 Sears had grown fine whisker of mercury, zinc, cadmium, silver and cadmium sulphide by this method, the

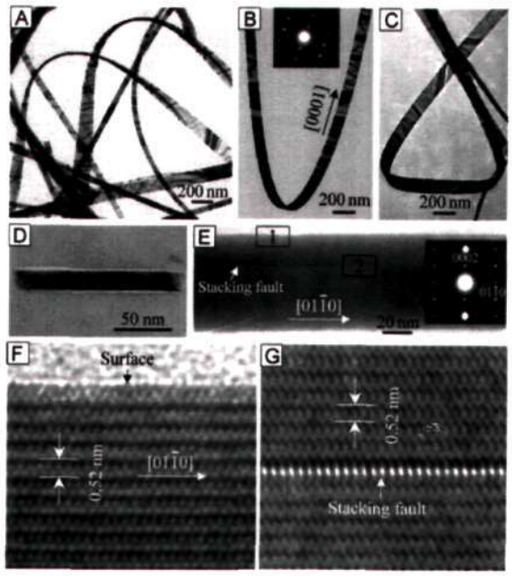

Figure 5. SEM and TEM pictures of ZnO nanobelts

growth process was explained by axial screw dislocation induced anisotropic growth.[31,32] Wang and his co-workers have grown the single crystal nanobelts of ZnO, SnO_2, In_2O_3 and CdO, by evaporating

the corresponding bulk metal oxides at high temperature under a vacuum and subsequently condensing the vapour on an alumina substrate, placed at relatively lower temperatures.[33] Figure 5 shows the SEM and TEM image of ZnO nanobelts obtained by Wang and his co-workers. Later on, number of people have employed this technique to generate wide variety of 1D nanomaterials, these includes left-handed helical nanostructure, nanorings and nanowires of ZnO, nanowires of Ga_2O_3, MgO, Al_2O_3, CuO and Si, nanorods of SnO_2 and nanobelts of PbO_2 and Ga_2O_3.[34-37]

In dissolution-condensation process, the growth species first dissolved into a solvent, and then diffuse through the liquid to deposit on the surface of growing nanostructures. The growth medium of dissolution-condensation process is different from

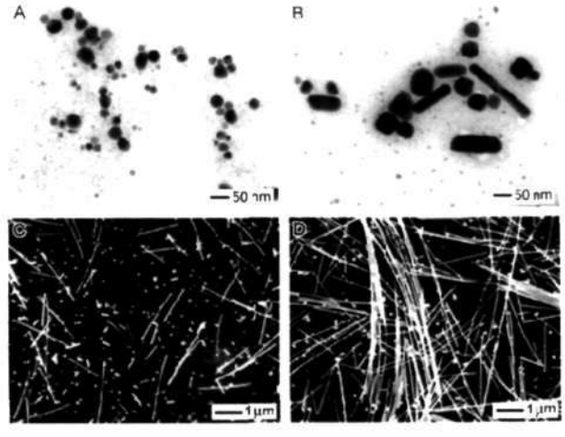

Figure 6. SEM images of silver nanowires grown in solution using Pt nanoparticles as growth seeds

evaporation-condensation process. Single crystalline nanowires of Se, Se_xTe_y, ZnTe, Mn_3O_4 and $BaTiO_4$, nanorods of $CdWO_4$ and ZnO and

nanotubes of $H_2Ti_3O_7$ have been obtained by this process.[38-41] In dissolution-condensation process alien nanoparticles can serve as seeds for heteroepitaxial growth of 1D nanomaterials. Ag nanowires of 30-40 nm in diameter with lengths of several tens of microns have been synthesised using platinum nanoparticles as growth seed.[45] The anisotropic growth was achieved by preferential blocking of specific facets by polyvinyl pyrrolidine (PVP). Figure 6 shows the Ag nanowires grown in solution using Pt nanoparticles as growth seeds.

1D nanomaterials obtained by the evaporation (dissolution)-condensation deposition usually have faceted morphology with small aspect ratios, particularly when grown in liquid medium. However, anisotropic growth induced by axial imperfections, such as screw dislocation and stacking faults, or by impurity poisoning, can result in the growth of nanowires with very large aspect ratios.

In Vapor-liquid-solid (VLS) growth the evaporated growth species diffuses and dissolves into a liquid droplet. The surface of the liquid

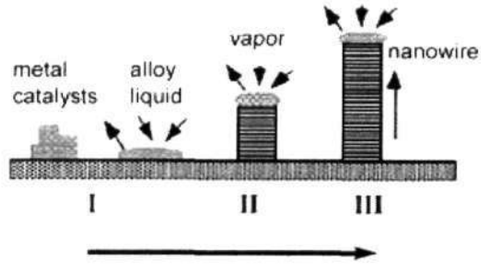

Figure 7. Schematic illustration showing the growth of a nanowires via VLS mechanism

has a large accommodation coefficient, and is therefore a preferred site for deposition. Saturated growth species in the liquid droplet will

diffuse to interface and precipitate at the interface between the substrate and the liquid. The precipitation will first follow nucleation then crystal growth. Continuous precipitation and growth will separate the substrate and the liquid droplet, resulting 1D growth of the nanomaterial. Figure 7 shows a schematic illustration showing the growth of a nanowire via VLS mechanism. The growth of Si and Ge nanowires with liquid gold droplets as catalyst are typical examples of VLS growth.[45,46] Nanowires of compound materials such as semiconductor nanowires of the III-V materials GaAs, GaP, GaAsP, InAs, InP, InAsP, the II-VI materials ZnS, ZnSe, CdS, CdSe and IV-IV alloys of SiGe have also grown using VLS method.[47]

Solution-liquid-solid (SLS) growth is similar to VLS growth but the reaction take place at solution phase and at relatively lower temperatures then VLS process. The SLS method was applied for the synthesis of InP, InAs, GaAs and Si nanowires.[48-50] The diameter and the lengths of nanowires grown by VLS and SLS methods can be controlled by controlling the size of the liquid catalysts and the growth time.

1D nanomaterials can also be synthesized by stress-induced recrystallization. Nanowires with diameter as small as 50 nm have been synthesised by applying pressure on solids at elevated temperature.[51] The growth rate of the nanowires was found to be proportional to applied pressure. Unlike other spontaneous growth processes, here growth proceeds from the base, not from the tip.

Dislocations at the base direct the uni-directional growth of the nanostructure.[52]

Template-based synthesis

Template-based synthesis is the most straightforward and versatile method in generating a wide range of nanomaterials. In this approach the template serve as a scaffold within which the required materials loaded and shaped into a morphology complimentary to that of template. This method has been used to fabricate a wide variety of nanomaterials like, nanorods, nanotubes, nanowires, nanohelics, nanosphere, naonobelts etc. Various templates have been explored for the growth of 1D nanomaterials. The most commonly used templates are anodized alumina membrane, radiation track-etched polymer membrane, mesoporous materials, zeolites and carbon nanotubes. These templates can be loaded with desired materials using either an electrodeposition route or by direct template filling.

Electrodeposition involves diffusion of precursors into the pores of the templates by applying an external electric field. In the next step, decomposition of the precursors and the deposition of growth species take place simultaneously. The resultant nanostructures can be harvested by removing the templates using a post-synthetic treatment such as chemical etching or calcination. A variety of 1D nanomaterials have been obtained by using this techniques, with typical examples as diverse as metals, semiconductors, ceramics and

organic polymers. Figure 8 shows an SEM image of CeO_2 nanotubes array obtained by the electrodeposition of $CeCl_3 \cdot 7H_2O$ into the pores of anodic alumina membranes.[53]

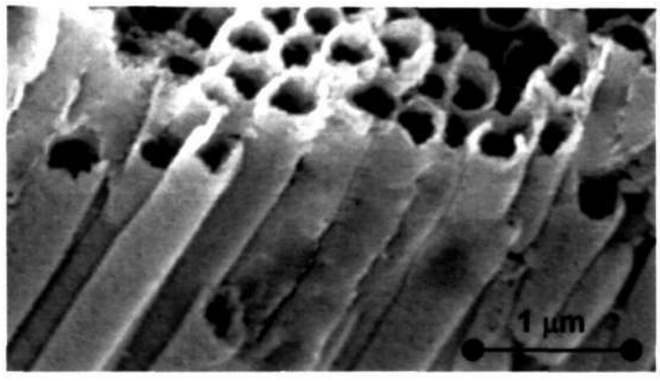

Figure 8. SEM image of the cross-sectional view of CeO_2 nanotubes

Direct template filling is the most popular methods in the preparation of 1D nanomaterials. The template can be filled with a liquid precursor or precursor mixture using techniques like sol-gel processing, melt and solution filling, chemical vapour deposition, centrifugation etc. In sol-gel processing the templates are placed in a stable sol for various periods of time to drive the sol into the pores by making use of capillary force. Good wetability of the templates surface for the sol is essential for this technique. After filling the pores templates are withdrawn and dried prior to the firing at elevated temperature. Figure 9 shows SEM image of nanotube arrays of $InVO_4$ and $InVO_4$–acac grown in polycarbonate templates by means of capillary force induced filling.[54]

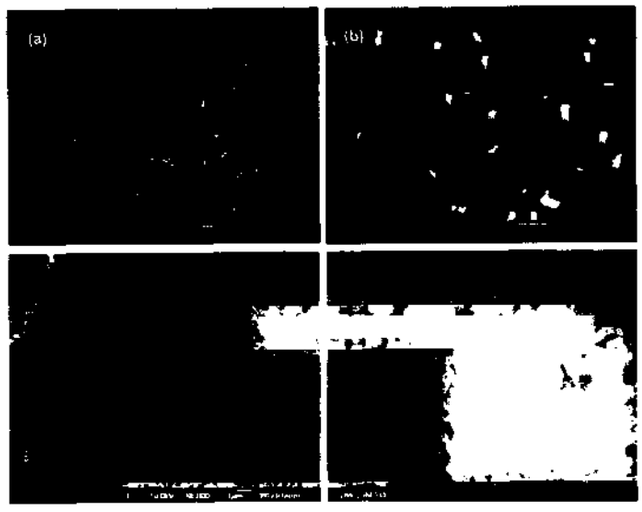

Figure 9: SEM images of (a) $InVO_4$ nanotube arrays, (b) magnified view of $InVO_4$ nanotube arrays, (c) $InVO_4$–acac nanotube arrays and (d) magnified view of $InVO_4$–acac nanotube arrays

Metals with relatively low melting points such as Bi, In, Sn and Al could be directly injected as liquids into the pores of anodic alumina membrane and subsequent solidification results into highly crystalline nanowires.[55,56] Polymer fibrils were prepared by filling a monomer solution with a polymerization reagent into the pores of a templates and then polymerizing the solution. Some researchers have also used chemical vapour deposition (CVD) to grow nanowires inside the pores of templates. For example, Ge nanowires were grown by diffusing Ge_2H_6 gas into the mesoporous silica at high temperature.[57] Template filling assisted with centrifugation is another inexpensive method for mass production of nanorod arrays. Nanorod arrays of lead zirconate titanate (PZT), silica and tiatania have been grown in

this method.[58] Although nanowires synthesized using these methods are usually polycrystalline, single crystal nanowires have also been obtained under carefully controlled conditions. Compound 1D nanomaterials can also be obtained using consumable templates. In this method first nanowires or nanorods of a constituent element is prepared, and then reacted with suitable reagents to form the compound nanomaterials.

Electrospinning

Electrospinning used electrical force to produce polymer fibers with nanometre scale dimensions. Electrospinning occurs when the electrical forces at the surface of polymer solution or melt overcome the surface tension and cause an electrically charged jet to be ejected. More than 30 polymer fibers with diameters ranging from 40 nm to 500 nm have been successfully produced by electrospinning.[59,60]

Lithography

Lithography represents another route to the synthesis of 1D nanomaterials. Various lithographic techniques such as electron beam lithgraphy, ion-beam lithography, STM lithography, X-ray lithography, proxial-probe lithography and near-field photolithography have been explored in the fabrication of nanomaterials.

1. 4. Two-dimensional nanomaterials

Two-dimensional (2D) nanomaterials such as nanowalls and nanosheets have at least one dimension in nanometer region. Unlike layered materials, nanosheets should be free from electrical and chemical interaction with other materials. The 2D nanomaterials are very exciting from the fundamental physics point of view and led to the discovery of new phenomena like quantum Hall effect[61,62] and giant magneto-resistance.[63,64] New devices such as high electron mobility transistors,[65] inter-sub-band infra-red detectors and quantum cascade lasers in semiconductor systems,[66] spin-valves in metallic systems[67] have been created based on these nanomaterials.

Several methods are being used for the preparation of two-dimensional nanomaterials that includes thermal exfoliation of layered materials, chemical vapour deposition (CVD), atomic layer deposition, physical vapour deposition, sol-gel processing and exploitation of the liquid-liquid interface.

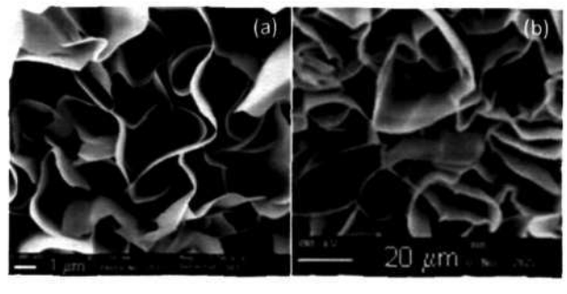

Figure 10. SEM image of the (a) GaS nanowalls (b) GaSe nanowalls

Thermal exfoliation method involves direct heating of the corresponding layered materials at required temperature. SEM image of GaS and GaSe nanowalls obtained by the thermal treatment of corresponding powder is shown in Figure 10.[68]

In chemical vapour deposition a volatile compound of the material to be deposited chemically reacts with other gases to produce a non-volatile solid that deposits atomistically on a substrate. A variety of CVD methods have been developed, depending on the types of precursors used, the deposition conditions applied and the forms of energy introduced to activate the chemical reactions. For example, when metal-organic compounds are used as precursors, the process is generally referred to as MOCVD (metalorganic CVD), when plasma is used to promote chemical reactions, this is a plasma enhanced CVD or PECVD and when low pressure applied this is called a low pressure CVD (LPCVD). Carbon nanowalls of thickness one to several nanometers have been grown on various substrates using microwave plasma-enhanced chemical vapour deposition.[69] Later on, this carbon nanowalls have been used as templates to obtain nanowalls of other inorganic materials, including Au, Cu, Zn, ZnO and TiO_2.

Atomic layer deposition (ALD) is a unique method for 2D nanomaterials having a self-limiting growth nature. In this method each time only one atomic or molecular layer can grow and so offers

the best possibility of controlling the thickness and the surface smoothness.

Physical vapour deposition involves transformations of the growth species to gaseous state followed by atomistic deposition on a suitable substrate. The process involves no chemical reactions. The thickness of the deposits can vary from angstroms to millimetres. In general, PVD methods can be divided into two groups: evaporation and sputtering. In evaporation, the growth species are removed from the source by thermal means. In sputtering, atoms or molecules are dislodged from solid target through the impact of gaseous ions (plasma).

Sol-gel processing, a widely used technique in the synthesis of inorganic and organic-inorganic hybrid materials are capable of producing nanomaterials of all dimensions. Most commonly used sol-gel methods for 2D nanomaterials are spin-coating and dip-coatings. In dip-coating, a substrate is immersed in a solution and then withdrawn at a constant speed. A spin coating consists of four stages: delivery of solution to the substrate centre, driving of the liquid across the substrate (spin-up), removal of the excess liquid from the substrate (spin-off) and evaporation. Number of polymer and polymer-composite thin-films have been grown by spin-coating.[70,71] Figure 11 shown the optical micrograph of an ultrathin organic–inorganic hybrid films with an interpenetrating network (IPN)

structure detached from the substrate and floating in ethanol, obtained by spin-coating method.

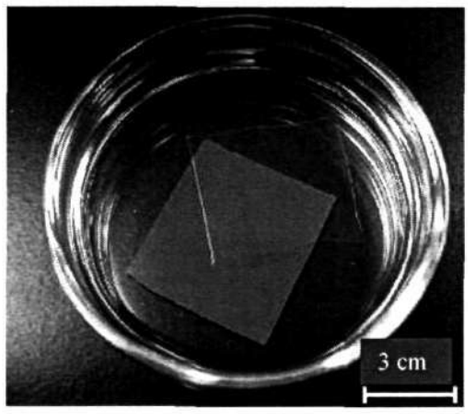

Figure 11. Optical micrograph of an IPN hybrid nanofilm detached from the substrate and floating in ethanol.

The liquid-liquid interface has also been exploited for the fabrication of 2D nanomaterials. The method involves dissolving an organic precursor of the relevant metal in the organic layer and the appropriate reagent in aqueous layer. The product formed by the reaction at the interface contains ultrathin nanocrystalline films. This simple technique has shown to yield nanocrystalline films of metals such as Au, Ag, Pd and Cu and chalcogenides such as CdS, CdSe, ZnS, CoS, NiS, CuS and PbS and oxides such as γ-Fe_2O_3, ZnO and CuO.[72-80]

A unique and perfect two dimensional material is graphene, a flat monolayer of carbon atoms in a closely packed honeycomb lattice. This basic building block of graphitic materials (fullerenes, carbon nanotubes and graphite) has a numbers of unique chemical,

physical and mechanical properties. Unlike other materials its charge carriers follow Dirac equation rather than the Schrodinger equation. It also exhibits unusual fractional quantum Hall effect and conductivity behaviour. Graphene is opening up a new research area for materials science and condensed-matter physics with a wide range of diversified potential applications. Despite the theoretical prediction of the thermodynamic unstability of a graphene sheet, a good number of efforts have been devoted to obtain good quality graphene samples.[81] Successful efforts include pyrolysis of camphor under reducing conditions,[82] exfoliation of graphitic oxide[83] and conversion of nanodiamond.[84]

References

1. T. Vossmeyer, L. Katsikas, M. Giersig, I. G. Popovic and H. Weller, *J. Phys. Chem.*, **98,** *7665*, 1994.

2. R. Zsigmondy, *Colloids and the Ultramicroscope*, J.Wiley and Sons, NY, 1914.

3. G. Binnig and H. Rohrer, *Rev Mod. Phys.*, **59**, *615*, 1987.

4. C. F. Hirjibehedin, C. Y. Lin, A. F. Otte, M. Ternes, C. P. Lutz, B. A. Jones and A. J. Heinrich, *Science,* **317,** *1199,* 2007.

5. A. P. Alivisatos, *Science,* **271,** *933*, 1996.

6. H. Yu, J. Li, R. A. Loomis, L. W. Wang and W. E. Buhro, *Nature Mater.,* **2,** *517,* 2003.

7. A. Mews, A. Eychmuller, M. Giersig, D. Schooss, H. Weller, *J. Phys. Chem.*, **98,** *934,* 1994.

8. C. N. R. Rao, G. U. Kulkarni, P. J. Thomas, and P. P. Edwards, *Chem. Eur. J.,* **8,** *28,* 2002.

9. L. Liu, Q. Peng, and Y. Li, *Inorg. Chem.*, **47**, *5022*, 2008.

10. G. Mie, *Ann. Phys.*, **25,** *377,* 1908.

11. G. C. Papavassilliou, *Prog. Solid State Chem.*, **12,** *185*, 1980.

12. R. Gans and *Ann. Phys.*, **31,** *881,* 1911.

13. R. Gans and *Ann. Phys.*, **47,** *270,* 1915.

14. S. V. Gaponenko, *Optical Properties of Semiconductor Nanocrystals, Cambridge* University Press, Cambridge 1998.

15. T. Vossmeyer, L. Katsikas, M. Giersig, *J. Phys. Chem.*, **98**, *7665*, 1994.

16. O. I. Micic, K. M. Jones and A. Cahill, *J. Phys. Chem. B,* **102,** *9791,* 1998.

17. L. E. Brus, *J. Chem. Phys.,* **79,** *5566,* 1983.

18. L. E. Brus, *J. Chem. Phys.,* **80,** *4403,* 1984.

19. T. Trindade, P. O. Brien and N. L. Pickett, *Chem. Mater.,* **13,** *3843,* 2001.

20. A. J. Sutherland, *Curr. Opin. Solid State Mater. Sci.,* **6**, *365,* 2002.

21. M. Bruchez, Jr., M. Moronne and P. Gin, *Science,* **281,** *2013,* 1998.

22. X. Peng, J. Wickham and A. P. Alivisatos, *J. Am. Chem. Soc.,* **120**, *5343,* 1998.

23. G. U. Kulkarni, P. J. Thomas, and C. N. R. Rao, *The Chemistry of Nanomaterials*, Wiley-VCH, Weinheim, 2004.

24. J. Park, J. Joo, S. G. Kwon, Y. Jang, and T. Hyeon, *Angew. Chem. Int. Ed.,* **46,** 4630, 2007.

25. C. Burda, X. Chen, R. Narayanan, and M. A. El-Sayed, *Chem. Rev.*, **105**, *1025,* 2005.

26. S. Iijima, *Nature,* **354**, *56,* 1991.

27. D. S. Bethune, C. H. Klang, M. S. D. Vries, G. Gorman, R. Savoy, J. Vazquez and R. Beyers, *Nature*, **363**, *605*, 1993.

28. Walt A. D. Heer, *Nature Mater.*, **1**, *153*, 2002.

29. A. Srivastava, O. N. Srivastava, S. Talapatra, R. Vajtai and P. M. Ajayan, *Nature Mater.*, **3,** *610*, 2004.

30. Guozhong Cao, *Nanostructures and Nanomaterials: Synthesis, Properties and Applications*, Imperial College Press, 2003.

31. G. W. Sears, *Acta Metal.*, **3,** *361*, 1955.

32. G. W. Sears, *Acta Metal.*, **3,** *367*, 1955.

33. Z. W. Pan, Z. R. Dai, and Z. L. Wang, *Science,* **291**, *1947* 2001.

34. X. Y. Kong and Z. L. Wang, *Nano Lett.*, **3**, *1625*, 2003.

35. X. Jiang, T. Herricks, and Y. Xia, *Nano Lett.*, **2**, *1333*, 2002.

36. P. Yang and C. M. Lieber, *Science*, **273,** *1836*, 1996.

37. W. Shi, H. Peng, Y. Zheng, N. Wang, N. Shang, Z. Pan, C. Lee, and S. Lee, *Adv. Mater.*, **12,** *1343*, 2000.

38. B. Gates, Y. Yin, and Y. Xia, *J Am. Chem. Soc.*, **122,** *12582*, 2000.

39. B. Mayers, B. Gates,Y. Yin, and Y. Xia, *Adv. Muter.*, **13,** *1380*, 2001.

40. Y. Li, Y. Ding, and Z. Wang, *Adv. Mater.*, **11**, *847*, 1999.

41. W. Wang, C. Xu, G. Wang, Y. Liu, and C. Zheng, *Adv. Mater.*, **14**, *837*, 2002.

42. J. J. Urban, W.S. Yun, Q. Gu, and H. Park, *J. Am. Chem. Soc.*, **124,** *1186*, 2002.

43. Q. Chen, W. Zhou, G. Du, and L. M. Peng, *Adv. Mater.*, **14,** *1208*, 2002.

44. Y. Sun, B. Gates, B. Mayers, and Y. Xia, *Nano Lett.*, **2,** *165*, 2002.

45. J. Hu, T. W. Odom, and C. M. Lieber, *Acc. Chem. Res.*, **32,** *435*, 1999.

46. A. M. Morales and C. M. Lieber, *Science*, **279**, *208* 1998.

47. X. Duan and C. M. Lieber, *Adv. Mater.*, **12**, *298*, 2000.

48. T. J. Trentler, K. M. Hickman, S. C. Goel, A. M. Viano, P. C. Gobbons, and W. E. Buhro, *Science*, **270**, *1791* 1995.

49. W. E. Buhro, *Polyhedron*, **13**, *1131* 1994.

50. H. Yu and W. E. Buhro, *Adv. Mater.*, **15**, *416*, 2003.

51. J. Franks, *Acta Metal.*, **6**, *103*, 1958.

52. J. D. Eshelby, *Phys. Rev.*, **91**, *775* 1953.

53. R. Inguanta, S. Piazza and C. Sunseri, *Nanotechnology*, **18**, *485605*, 2007.

54. Y. Wang and G. Cao, *J. Mater. Chem.*, **17**, *894*, 2007.

55. Z. Zhang, D. Gekhtman, M. S. Dresselhaus, and J. Y. Ying, *Chem. Mater.*, **11**, *1659*, 1999.

56. E. G. Wolfe and T. D. Coskren, *J. Am. Ceram. Soc.*, **48**, *279* 1965.

57. X. Duan and C. M. Lieber, *Adv. Mater.*, **12**, *298*, 2000.

58. T. Wen, J. Zhang, T. P. Chou, and G. Z. Cao, *J. Sol-Gel Sci. Technol.*, **33**, *193*, 2005.

59. H. Fong, W. Liu, C. S. Wang, and R. A. Vaia, *Polymer*, **43**, *775*, 2002.

60. J. A. Mathews, G. E. Wnek, D. G. Simpson, and G. L. Bowlin, *Biomacromolecules*, **3**, *232*, 2002.

61. K. V. Klitzing, G. Dorda, and M. Pepper, *Phys. Rev. Lett.*, **33**, *827*, 1980.

62. D. Tsui, and H. Stormer, *IEEE J. Quantum Electron.*, **22**, *1711*, 1986.

63. M. N. Baibich, J. M. Broto, A. Fert, F. Nguyen V. Dau, F. Petroff, P. Etienne, G. Creuzet, A. Friederich and J. Chazelas, *Phys. Rev. Lett.*, **61**, *2472*, 1988.

64. G. Binasch, P. Grunberg, F. Saurenbach and W. Zinn, *Phys. Rev. B*, **39**, *4828*, 1989.

65. M. Abe, T. Mimura, K. Nishiuchi, A. Shibatomi and M. Kobayashi *IEEE J. Quantum Electron.*, **22**, *1870*, 1986..

66. J. Faist, F. Capasso, D. L. Sivco, C. Sirtori, A. L. Hutchinson, and A. Y. Cho, *Science,* **264,** *553,* 1994.

67. B. Dieny, V. S. Speriosu, S. S. P. Parkin, B. A. Gurney, D. R. Wilhoit and D. Mauri, *Phys. Rev. B,* **43,** *1297,* 1991.

68. U. K. Gautam, S. R. C. Vivekchand, A. Govindaraj and C. N. R. Rao, *Chem. Commun., 3995*, 2005.

69. Y. Wu, B. Yang, B. Zong, H. Sun, Z. Shen and Y. Feng, *J. Mater. Chem.*, **14**, *469*, 2004.

70. R. Vendamme, S. Onoue, A. Nakao and T. Kunitake, *Nat. Mater.*, **5**, *494*, 2006.

71. H. Watanabe and T. Kunitake, *Adv. Mater.*, **19**, *909*, 2007.

72. C. N. R. Rao, G. U. Kulkarni, V. V. Agrawal, U. K. Gautam, M. Ghosh and U. Tumkurkar, *J. Colloid Interface Sci.*, **289**, *305*, 2005.

73. C. N. R. Rao, G. U. Kulkarni, P. J. Thomas, V. V. Agarwal and P. Saravanan, *Curr. Sci.*, **85**, *1041*, 2003.

74. Y. Lin, H. Skaff, T. Emrick, A.D. Dinsmore and T. P. Russell, *Science,*

299, *226*, 2003.

75. C. N. R. Rao, G. U. Kulkarni, P. J. Thomas, V. V. Agarwal and P. Saravanan, *J. Phys. Chem. B*, **107**, *7391*, 2003.

76. V. V. Agrawal, G. U. Kulkarni and C. N. R. Rao, *J. Phys. Chem. B*, **109**, *7300*, 2005.

77. V. V. Agrawal, P. Mahalakshmi, G. U. Kulkarni and C. N. R. Rao, *Langmuir*, **22**, 1846, 2006.

78. U. K. Gautam,M. Ghosh and C. N. R. Rao, *Chem. Phys. Lett.*, **381**, *1*, 2003.

79. U. K. Gautam, M. Ghosh and C. N. R. Rao, *Langmuir*, **20**, *10775*, 2004.

80. K. P. Kalyanikutty, U. K. Gautam and C. N. R. Rao, *Solid State Sci.*,

8, *296*, 2006.

80. K. P. Kalyanikutty, U. K. Gautam and C. N. R. Rao, *J. Nanosci. Nanotechnol.*, **7**, *1916*, 2007.

81. K. S. Subrahmanyam, S. R. C. Vivekchand, A. Govindaraj and C. N. R. Rao, *J. Mater. Chem.*, **18**, *1517*, 2008,

82. P. R. Somani, S. P. Somani and M. Umeno, *Chem. Phys. Lett.*, **430**, *56*, 2006.

83. H. C. Schniepp, J. L. Li, M. J. McAllister, H. Sai, M. H. Alonso, D. H. Adamson, R. K. Prudhomme, R. Car, D. A. Saville and I. A. Aksay, *J. Phys. Chem. B*, **110**, *8535*, 2006.

84. O. E. Andersson, B. L. V. Prasad, H. Sato, T. Enoki, Y. Hishiyama, Y. Kaburagi, M. Yoshikawa and S. Bandow, *Phys. Rev. B*, **58,** *16387*, 1998.

CHAPTER 2

Synthesis and characterization of metal oxide nanorod brushes

Summary

This chapter of the thesis deals with the synthesis and characterization of metal oxides nanorod brushes. Nanorod brushes of α-Al_2O_3, MoO_3 and ZnO have been synthesized using amorphous carbon nanotube (a-CNT) brushes as the starting material. Nanobrushes of α-Al_2O_3 and MoO_3 are made up of single crystalline nanorods. In the case of ZnO nanobrushes, the nanorod bristles are made by the fusion of 15 to 25 nm size nanoparticles and are porous in nature. Metal oxide nanorod brushes thus obtained have been characterized by XRD, FESEM, TEM and Raman spectroscopy. Single crystalline ruby nanorods were obtained by introducing chromium ions during the synthesis of alumina rods.

A paper based on this study has been published in *Bull. Mater. Sci.*, **(2008)**.

2.1 Introduction

Avid attention has been given to the preparation of one-dimensional inorganic nanomaterials with different morphologies, such as nanotubes, nanorods and nanohelics.[1] Special attention has been paid to the metal oxide nanorods because of their improved properties compared to their bulk-counterparts. For many technological applications it is highly desirable to produced nanorods in brush morphology covering a large area. These nanorod brushes are also important for the understanding of fundamental physical concepts.

Aluminium oxides are remarkable materials with broad applicability in the chemical and petrochemical industry as adsorbents, catalyst supports or as a part of bifunctional catalysts. These oxides have also been utilised as capacitor dielectrics and gate oxides in memory device owing to its high dielectric constant, very low permeability, and high thermal conductivity.[2-4] Currently nano-structured aluminas including nanowires, nanotubes, and nanorods are in the focus of both academic and industrial research, because of their interesting one dimensional characteristics and possible applications in nanomaterials-based electronics.

Orthorhombic molybdenum trioxide (α-MoO_3), a wide-gap, n-type semiconductor material, has attracted considerable interest due to its layered crystal structures and wide applications in electronic

display systems, solid state microbatteries, gas sensors and recording materials.[5-7] It is one of the most widely used catalysts for selective oxidation reactions in petroleum refinery, chemical production and pollution control industries.[8] In α-MoO_3 the asymmetrical MoO_6 octahedra are interconnected through corner-linking along [100] and edge-sharing along [001] to form double-layer sheets parallel to the (010) plane. The weak interactions between the double-layer sheets are mostly van der Waals forces.[9] Nanostructures of MoO_3 can find applications in lubricants,[10,11] sensors,[12,13] rechargeable lithium-ion batteries,[14] and field emission nanodevices.[15-17]

Zinc oxide is a direct and wide band gap (3.37 eV) semiconductor with a large exciton binding energy (60 meV). It is one of the most interesting functional materials with a number of unique properties like transparent conductivity, near-UV emission,[18] UV absorption,[19] field-emission capabilities[20] and piezoelectricity. Due to its unique properties nanomaterials of ZnO stimulates a wide range of research interest. As a result ZnO has been synthesized in variety of attractive morphologies including nanotubes, nanowires, nanohelics, nanonails, nanobowls and nanoflowers. One-dimensional nanostructures of ZnO are promising materials in number of potential applications like in gas sensors,[21,22] solar cells,[23] nanolasers[24] and transparent ultraviolet protection film.

2.2 Scope of the present study

Synthesis of one dimensional metal oxide nanostructures is getting enormous attention in recent years due to their potential applications in nanoelectronics, photonics, data recording media, gas sensing and gas storage.[1] Though several transition metal oxides in the form of wires, tubes and rods were reported using various chemical and physical methods, synthesis of Al_2O_3 and MoO_3 nanorods has generated a great deal of interest owing to their improved mechanical and catalytic behaviour, nonlinear optical characteristics and unusual optical luminescence properties. Various approaches to synthesize these metal oxide nanorods involve vapour-liquid-solid growth, vapour-solid growth, laser ablation, solvothermal, electrochemical and carbothermal methods.[1,25] Al_2O_3 nanowires were obtained by vapor-liquid-solid growth in presence of SiO_2 and Fe act as catalyst.[26-29] Rao et al[30,31] synthesized crystalline γ-Al_2O_3 and MoO_3 nanotubes through carbothermal route by coating the functionalized carbon nanotubes with aluminum iso-propoxide. In a similar approach, Li et al[32] reported the formation of single crystalline alumina using mesoporous carbon aerogels as substrate and aluminum nitrate as the source. Short alumina naotubes have also been fabricated by controlling anodization process of aluminum in dilute sulfuric acid.[33,34] Xiao et al,[35] electrodeposited alumina inside the pores of alumina membrane and finally etch out the membrane using aqueous NaOH solution to obtain alumina

nanotubes and nanowires. Lee et al,[36] synthesized alumina nanowires by hydrothermal method in presence of surfactants. α-Al_2O_3 nanobelts and nanosheets with different morphologies and size have been prepared by a chemical route from H_2O and Al in argon atmosphere at high temperatures.[37] Kim and co-workers synthesized amorphous Al_2O_3 nanotubes by atomic layer deposition of alumina on ZnO core followed by etching the ZnO.[38] Indeed, similar methods were adopted for the preparation of MoO_3 nanowires and nanotubes by several researchers.[39-42] In all these cases the one-dimensional morphologies obtained for Al_2O_3 and MoO_3 was mostly restricted to tubular and fibrous structures and no formation of aligned, single-crystalline nanorods were reported so far by any chemical route. In this report we have synthesized crystalline Al_2O_3, MoO_3 and ZnO nanorod brushes using amorphous carbon nanotube (a-CNT) brushes as the starting materials. Amorphous carbon nanotube brushes[43] were derived from the carbonization of glucose within the polycarbonate membranes. By introducing chromium during the synthesis of alumina nanorods we have also obtained single crystalline ruby nanorod brushes.

2.3 Experimental and related aspects

Synthesis

a-CNT brushes

Amorphous carbon nanotube (a-CNT) brushes were prepared by the following procedure.[43] Polycarbonate membranes with a pore diameter of 220 nm were soaked in 22 mL of 0.5 M aqueous solution of glucose in a 25 mL Teflon-lined autoclave. The temperature of the autoclave was maintained at 180 °C for 6 h after which it was allowed to cool to room temperature. The brownish liquid, rich in carbon spheres was discarded. The membranes that had turned brown were washed with deionized water and ethanol several times and dried at 40 °C for 1 h.

Metal oxide nanorod brushes

To obtain Al_2O_3 nanorods, the brown coloured membrane was first soaked in 0.5 M solution of aluminum nitrate nanohydrate for 12 h and then dried at 45°C for 5 h. The composite was further heated at 1100 °C for 3 h to give white- coloured Al_2O_3 nanorods. Pink coloured ruby nanorods were prepared by introducing 0.25 g (Cr/Al = 0.025) chromium nitrate nanohydrate along with the aluminum nitrate precursor during the synthesis. For MoO_3 rods, the membrane was soaked in the 0.028 M solution of ammonium heptamolybdate tetrahydrate for 12 h followed by drying at 45 °C for 5 h. In the case of ZnO nanorods, 0.5 M solution of zinc nitrate was

used. The Zn and Mo precursor loaded composite membranes were thermally treated at 430 °C for 3 h to obtain bluish- coloured MoO_3 and white coloured ZnO nanorod brushes. The products were investigated by electron microscopy and other physical techniques.

Characterization Techniques

X-ray diffraction (XRD): X-ray diffraction patterns of nanorod brushes were recorded at 25 °C with a Rich-Siefert 3000-TT diffractometer employing Cu Kα radiation.

Scanning Electron Microscopy (SEM): The morphology of the nanotubes was examined by a Field Emission Scanning Electron Microscope (FESEM, FEI Nova-Nano SEM-600, Netherlands), and scanning electron microscope (SEM) Leica S-440I instrument (U.K).

Transmission Electron Microscopy (TEM): TEM images were recorded with a JEOL JEM 3010 instrument (Japan) operated at an accelerating voltage of 300 kV.

Raman spectroscopy: Raman spectra were recorded with a LabRAM HR with 633 nm line from HeNe laser.

Photoluminescence: Photoluminescence studies were done by using Perkin Elmer LS 50B instrument using a Xe lamp source.

2.4 Results and discussion

Amorphous carbon nanotube (a-CNT) brushes

In Figure 1a we show a FESEM image of a-CNTs, after dissolution of polycarbonate membrane using dichloromethane. All the nanotubes are well aligned and packed together as brushes. The length of the nanotube is around 15 μm. The outer diameter of the nanotube is around 250 nm with the wall thickness of 45 nm (Figure 1b).

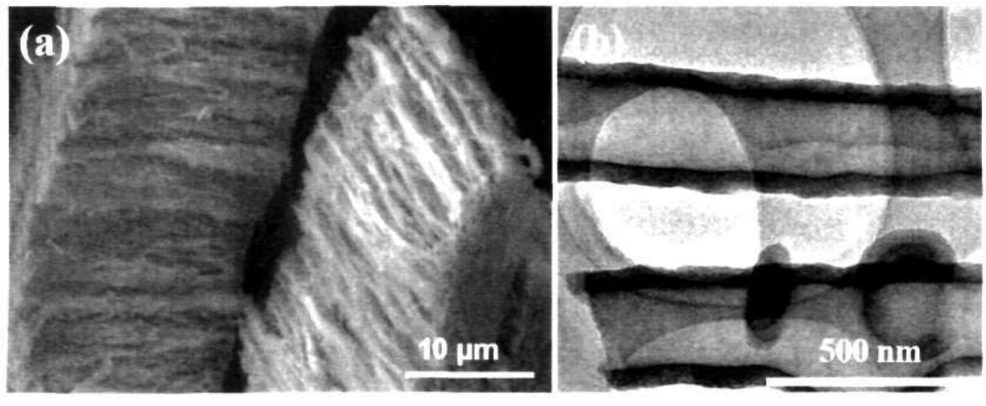

Figure 1: (a) FESEM image of a-CNTs (b) TEM image of a-CNTs

α-Al_2O_3 nanorod brushes

Calcination of amorphous carbon membrane filled with aluminum precursor at high temperature (1100 °C) yields crystalline alumina nanorods with brush like morphology analogous to a-CNT brushes. Figure 2a shows a low magnification FESEM image of α-Al_2O_3 nanorods in which all the nanorods are well aligned and

packed together covering a large area. The high magnification FESEM image of the rods in Figure 2b, viewed perpendicular to the rod axis, shows a smooth surface with occasional joints all along their length indicating the end to end fusion of alumina nanorods of 1 μm length.

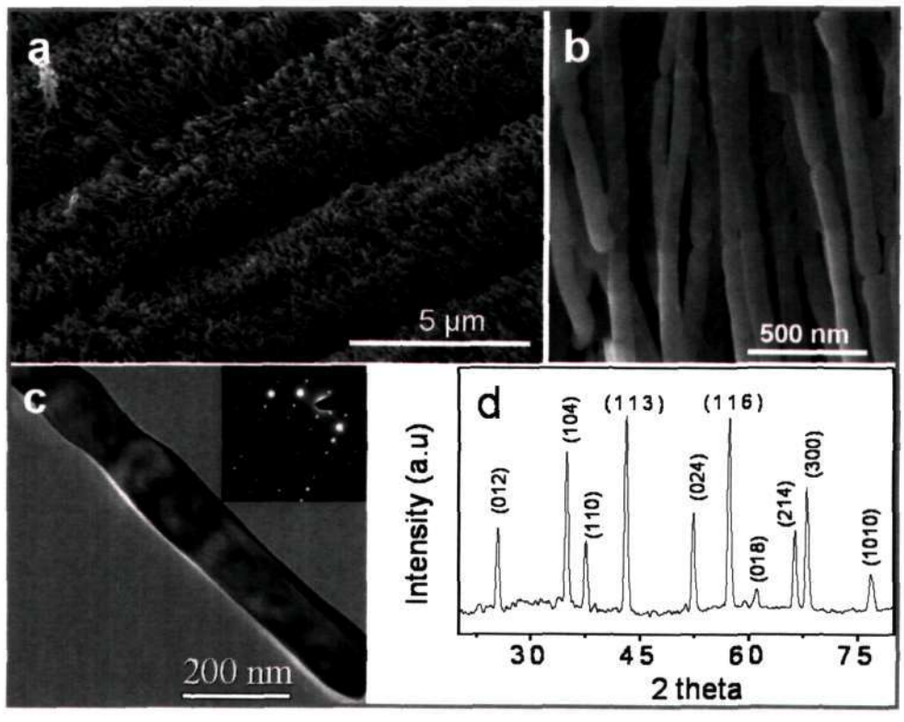

Figure 2: (a) FESEM image of α-Al_2O_3 nanorods (b) Higher magnification FESEM image of α-Al_2O_3 nanorods (c) TEM image of a individual α-Al_2O_3 nanorods (d) XRD of α-Al_2O_3 nanorods

A TEM image of an individual nanorod shown in Figure 2c reveals that the diameter of the tube is around 150 nm. Inset of Figure 2c is the corresponding electron diffraction pattern revealing the single crystalline nature of the nanorods. The XRD pattern of the Al_2O_3 nanorods shows all the reflections indexed to pure α-Al_2O_3 corundum

structures with cell parameter a = 4.758Å and b = 12.99Å (JCPDF card No: 461212). The sharp peaks in the XRD pattern reflect the crystalline nature of the nanorods, supporting the electron diffraction pattern.

Ruby nanorod brushes

Cr doped single crystalline α-Al_2O_3, (ruby) is the first solid state laser invented in 1960.[44] Ruby is still used in number of applications where short pulse of red light is required. Ruby produces a pulse of visible light with a wavelength of 694 nm. Nanorods of ruby were not reported hitherto. We have obtained single crystalline ruby nanorods by introducing chromium ions during the

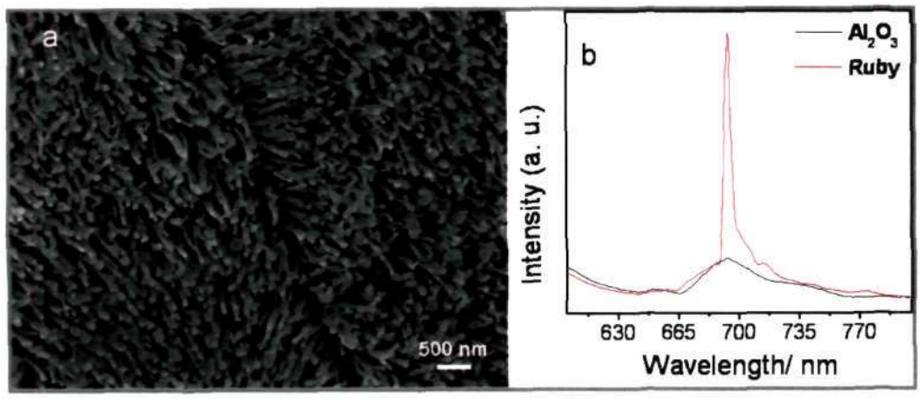

Figure 3: (a) FESEM image of ruby nanorods (b) PL spectra of ruby and alumina nanorods

synthesis of single crystalline alumina rods. A FESEM image of well-aligned ruby nanorods is shown in Figure 3a. In Figure 3b the photoluminescence properties of the ruby nanorods is compared with the α-Al_2O_3 nanorods. The intense PL peak of ruby nanorods at 693.5

nm is several times stronger than the α-Al_2O_3 nanorods. In addition it shows a very sharp emission peak, with narrow bandwidth as against the broad emission peak for alumina. The characteristic R1 and R2 peaks of ruby merge to a single peak due to temperature broadening and low-resolution power of the instrument.

MoO_3 nanorod brushes

In Figure 4a we show a FESEM image of MoO_3 nanorods exhibiting brush like morphology similar to that of a-CNTs brush template. The average diameter of the nanorods is around 190 nm.

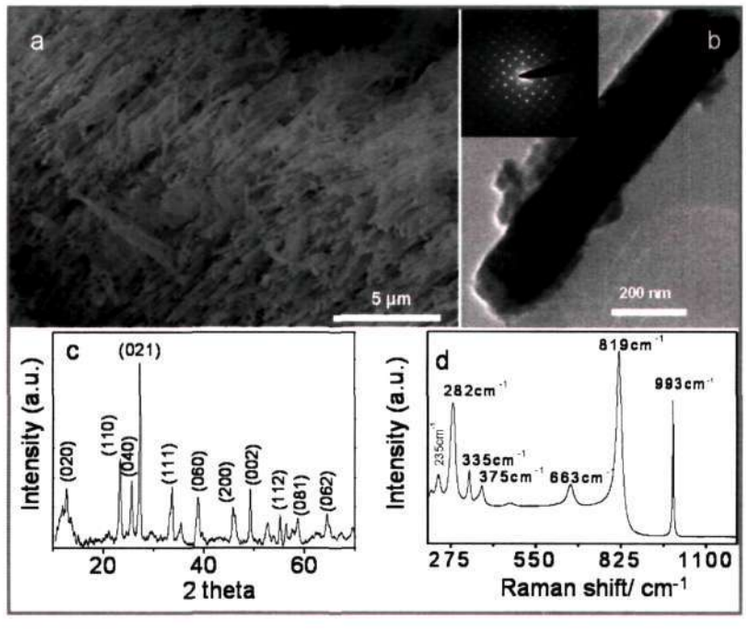

Figure 4: (a) FESEM image of MoO_3 nanorods (b) TEM image of a individual MoO_3 nanorod (c) XRD pattern of MoO_3 nanorods (d) Raman spectra of MoO_3 nanorods

The length of the nanorods is less than 2 µm and is not upto the thickness of the membrane suggesting the discontinuity in the structure. TEM image shown in Figure 4b confirms the rod like

morphology of MoO_3. The electron diffraction pattern shown in the inset of Figure 4b indicates that the nanorods were single crystalline. Figure 4c shows the XRD pattern of MoO_3, the strong intensity of the peaks indicates the high crystallinity of the nanorods. All the peaks can be indexed to the pure phase of α-MoO_3 with the orthorhombic structure and lattice parameters are a = 3.96 Å, b = 13.86 Å and c = 3.7 Å (JCPDS card number 05-0508). The nanorods show the characteristics Raman bands for the MoO_3 crystal (Figure 4d) at 235(B_{3g}), 282(B_{2g}, B_{3g}), 335(B_{1g}, A_g), 375(B_{1g}), 663(B_{2g}, B_{3g}), 819(A_g, B_{1g}) and 993(A_g, B_{1g}) cm^{-1}.

ZnO nanorod brushes

Figure 5a shows a FESEM image of aligned ZnO nanorods obtained through the a-CNT template. In contrast to Al_2O_3 and MoO_3, ZnO nanorods are made up of small nanoparticles of around 15 to 25 nm diameter. The diameter of the nanorods is in the range of 150 to 180 nm with lengths of about 15 μm. TEM image shows that nanoparticles are fused randomly to form a nanoporous rod. The Electron diffraction pattern shown in the inset of Figure 5b confirms the polycrystalline nature of the nanorods. The broad peaks observed in the XRD pattern further support our observation that the nanorods are composed of ZnO nanoparticles. These porous nanostructures might have high surface area with good potential applications.

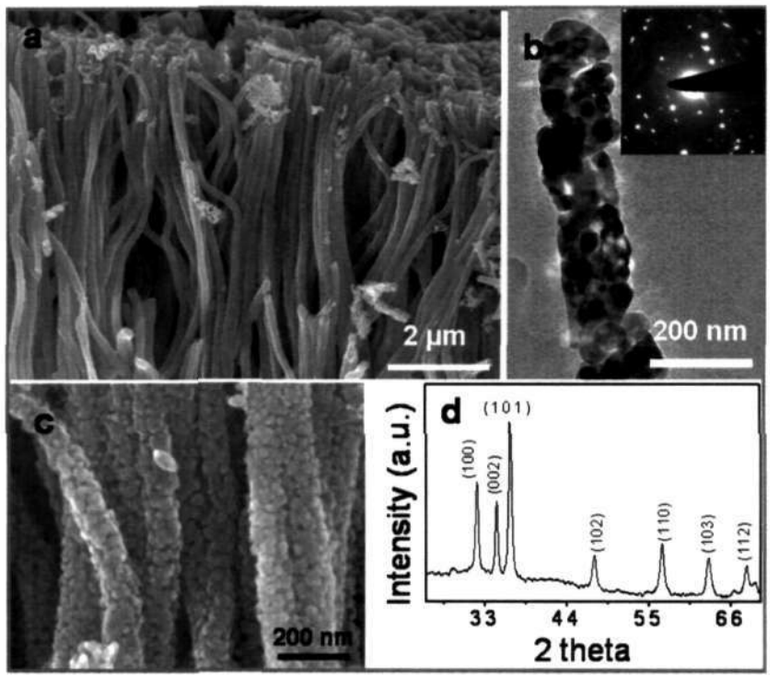

Figure 5: (a) FESEM image of ZnO nanorods (b) Higher magnification FSESEM image of ZnO nanorods(c) TEM Image of an individual ZnO nanorod (inset ED pattern on the nanorod) (d) XRD pattern of ZnO nanorods

2.5 Conclusions

In conclusion, we have utilized the amorphous carbon nanotube brushes as template to prepare single crystalline nanorod brushes of Al_2O_3 and MoO_3 and polycrystalline brushes of ZnO. We believe that the presence of carboxylic and phenolic functional groups present on the surface of the a-CNT helps to hydrolyze the metal precursors within the voids of the membrane which would subsequently form a polymer network (Scheme 1). Further calcination at high temperatures, coupled with the exothermic heat generated by the combustion of carbon facilitates the formation of crystalline nanorods of metal oxides.

References

1. C. N. R. Rao and A. Govindaraj, Nanotubes and Nanowires, Cambridge RSC Publishing, 2005.

2. Y. Kim, S. M. Lee, C. S. Park, S. I. Lee and M. Y. Lee, *Appl. Phys. Lett.*, **71**, *3604*, 1997.

3. W. S. Jeon, S. Yang, C. S. Lee and S. W. Kang, *J. Electrochem. Soc.*, **149,** *C306,* 2002.

4. E. P. Gusev, M. Copel, E. Cartier, I. J. R. Baumvol, C. Krug and M. A. Gribelyuk, *Appl. Phys. Lett.*, **76**, *176,* 2000.

5. Z. Hussain, *J. Mater. Res.* **16**, *2695,* 2001.

6. M. Ferroni, V. Guidi, G. Martinelli, M. Sacerdoti, P. Nelli, and G. Sberveglieri, *Sens. Actuators B,* **48**, *285,* 1998.

7. H. C. Zeng, *Inorg. Chem.* **37**, *1967,* 1998.

8. H. F. Liu, R. S. Liu, K. Y. Liew, R. E. Johnson and J. H. Lunsford, *J. Am. Chem. Soc.*, **106**, *4117,* 1984.

9. X. W. Lou and H. C. Zeng, *Chem. Mater,* **14**, *4781,* 2002.

10. P. E. Sheehan and C. M. Lieber, *Science*, **272,** *1158,* 1996.

11. J. Wang, K. C. Rose and C. M. Lieber, *J. Phys. Chem. B,* **103**, *8405,* 1999.

12. E. Comini, L. Yubao, Y. Brando and G. Sberveglieri, *Chem. Phys. Lett.*, **407**, *368,* 2005.

13. A. M. Taurino, A. Forleo, L. Francioso, P. Siciliano, M. Stalder and R. Nesper, *Appl. Phys. Lett.*, **88**, *15211*, 2006.

14. W. Li, F. Cheng, Z. Tao and J. Chen, *J. Phys. Chem. B*, **110**, *119*, 2006.

15. Y. B. Li, Y. Bando, D. Golberg and K. Kurashima, *Appl. Phys. Lett.*, **81**, *5048*, 2002.

16. J. Zhou, S. Z. Deng, N. S. Xu, J. Chen and J. C. She, *Appl. Phys. Lett.*, **83**, *2653*, 2003.

17. J. Zhou, N. S. Xu, S. Z. Deng, J. Chen, J. C. She and Z. L. Wang, *Adv. Mater.*, **15,** *1835*, 2003.

18. R. E. Service, *Science*, **276**, *895*, 1997.

19. E. A. Meulenkamp, *J. Phys. Chem. B*, **102**, *5566*, 1998.

20. D. Banerjee, S. H. Jo and Z. F. Ren, *Adv. Mater.*, **16**, *2028*, 2004.

21. J. Hu, T. W. Odom and C. M. Leiber, *Acc. Chem. Res.*, **32**, *435*, 1999.

22. N. J. Dayan, S. R. Sainkar, R. N. Karekar, and R. C. Aiyer, *Thin Solid Films*, **325,** 254, 1998.

23. Z. W. Pang, Z. R. Dai and Z. L. Wang, *Science*, **291,** *1949*, 2001.

24. M. H. Huang, S. Mao, H. Feick, H. Q. Yan, Y. Y. Wu, H. Kind, E. Weber, R. Russo and P. D. Yang, *Science*, **292**, *1897*, 2001.

25. C. N. R. Rao, S. R. C. Vivekchand, K . Biswas and A. Govindaraj, *Dalton Trans.*, **34**, *3728*, 2007.

26. V. Valcarcel, A. Souto and F. Guitian, *Adv. Mater.*, **10**, *138,* 1998.

27. C. C. Tang, S. S. Fan, P. Li, L. Chapelle, and H. Y. Dang, *J. Crystal Growth*, **224,** *117*, 2001.

28. X. S. Peng, L. D. Meng, X. F. Wang, C. Z. Wang, and G. S. Wu, *J. Phys. Chem. B,* **106,** *11163*, 2003.

29. J. Zhou, S. Z. Deng, J. C. She and N. S. Xu, *Chem. Phys. Lett.*, **365**, *505*, 2002.

30. B. C. Satishkumar, A. Govindaraj, E. M. Vogl, L. Basmallick and C. N. R. Rao, *J. Mater. Res.*, **12**, *604*, 1997.

31. B. C. Satishkumar, A. Govindaraj, M. Nath and C. N. R. Rao, *J. Mater. Chem.*,**10,** *2115*, 2002.

32. W. Li, A. H. Lu, C. Weidenthaler, R. Goddard, H. J. Bongard and F. Schuth, *J. Mater. Chem.*, **15**, *2993*, 2005.

33. L. Pu, X. Bao, J. Zou, and D. Feng, *Angew. Chem. Int. Ed*, **40**, *1490*, 2001.

34. J. Zou, L. Pu, X. Bao, and D. Feng, *Appl. Phys. Lett.*, **80**, *1079*, 2002.

35. Z. L. Xiao, C. Y. Han, U. Welp, H. H. Wang, W. K. Kwok, G. A. Willing, J. M. Hiller, R. E. Cook, D. J. Miller, and G. W. Crabtree, *Nano Lett.*, **2,** *1293*, 2002.

36. H. C. Lee, H. J. Kim, S. H. Chung, K. H. Lee, H. C. Lee and J. S. Lee, *J. Am. Chem. Soc.*, **125**, *2882*, 2003.

37. X. S. Fang, C. H. Ye, X. S. Peng, Y. H. Wang, Y. C. Wu and. L. D. Zhang, *J. Mater. Chem.*, **13,** *3040*, 2003.

38. J. Hwang, B. Min, J. S. Lee, K. Keem, K. Cho, M. Y. Sung, M. S. Lee and S. Kim, *Adv. Mater.*, **16**, *422*, 2004.

39. X. W. Lou and H. C. Zeng, *Chem. Mater.*, **14**, *4781*, 2002.

40. T. Xia, Q. Li, X. Liu, J. Meng and X. Cao, *J. Phys. Chem. B*, **110** *2006*, 2006.

41. R. Q. Song, A. W. Xu, B. Deng, and Y. P. Fang, *J. Phys. Chem. B*, **109**, *22758*, 2005.

42. N. Niederberger, F. Krumeich, H. J. Muhr, M. M. Llerb and R. Nesper, *J. Mater. Chem.*, **11**, *1941*, 2001.

43. J. Dinesh, M. Eswaramoorthy and C. N. R. Rao, *J. Phys. Chem. C*, **111,** *510*, 2007.

44. T. H. Mayman, *Nature*, **187**, *493*, 1960.

CHAPTER 3

Synthesis, structure and properties of homogeneous BC_4N nanotubes

Summary

This chapter of the thesis deals with the synthesis, characterization and properties of boron carbon nitride (BCN) nanotube brushes. BCN nanotube brushes were obtained by the high temperature reaction of amorphous carbon nanotube (a-CNT) brushes with a mixture of boric acid and urea. The a-CNT brushes themselves were obtained by the pyrolysis of glucose in a polycarbonate membrane. BCN nanotubes have been characterized by EELS, XPS, electron microscopy, Raman spectroscopy and other techniques. The composition of the BCN nanotubes is found to be BC_4N by X-ray photoelectron spectroscopy and electron energy loss spectroscopy. The BC_4N nanotubes, which are stable upto 900 °C, are insulating and nonmagnetic. They exhibit a selective uptake of CO_2 upto 23.5 wt %.

A paper based on this work has been published in Journal of Materials Chemistry (**2008**).

3.1 Introduction

Boron carbon nitrides (BCN) are important materials with a variety of attractive properties and applications. The idea of BCN materials originates from the structural similarity but quite different

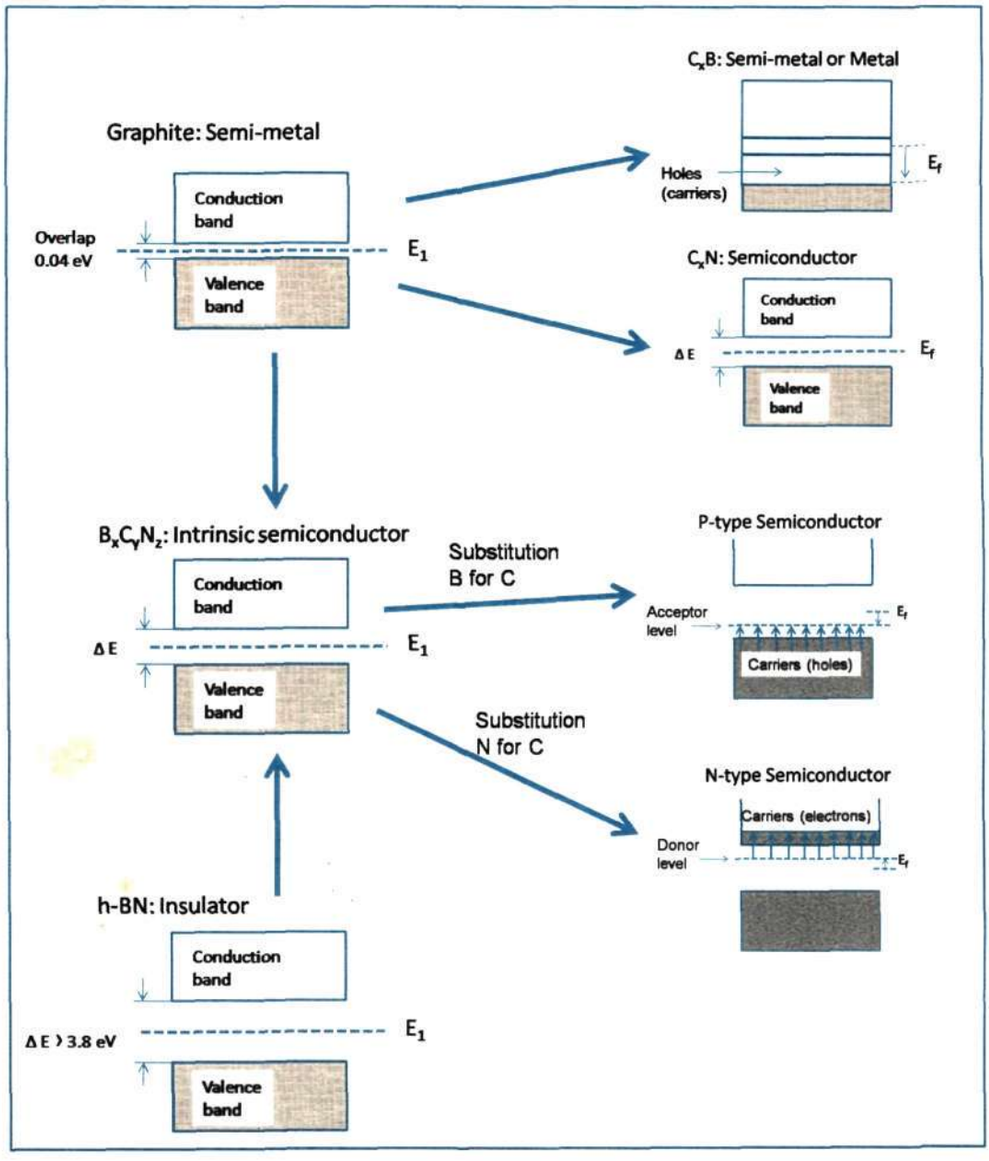

Figure 1: The expected band structure of BCN materials.

properties of graphite and hexagonal boron nitride (h-BN).[1] h-BN is an insulator having limited intercalation properties while graphite is an excellant host material with semi-metallic conductivity. The properties of BCN materials can be expected to be in between those of graphite and h-BN. For example several types of semiconductors were obtained for BCN materials of different compositions as shown in the schematic in figure 1. One is an intrinsic type BCN semiconductor which can be converted to a p-type or an n-type extrinsic semiconductor by replacing carbon with boron or nitrogen, respectively. The band gap of intrinsic type BCN semiconductor depends on both composition as well as atomic configuration in the layers.

Number of other interesting properties, like luminesence, intercalation, lubrication, neutron absorption, thermoelectricity and rectification are associated with these BCN materials. The nanostructures of these materials have even improved properties and broader applicability.[2] For example, the luminescence propreties associated with BCN nanotubes could find applications in electroluminesence and light-emitting diodes.[3-5] Similarly, the excellent intercalation properties could be exploited for electrode matrix for secondary lithium batteries, molecular sieves, gas storage and catalysis.[6]

3.2 Scope of the present study

The fascinating properties of carbon nanotubes[7] gave enormous impetus to researchers to explore analogous materials such as boron nitride (BN), boron carbon nitride (BCN) and boron carbide (BC) nanotubes. Out of these, BCN nanotubes attracted considerable interest because of their attractive properties which can be tuned by varying their composition and the arrangement of B, C and N atoms. Stephen et al,[8] first reported carbon nanotubes containing B and N prepared through a modified electric arc-discharge method turns out to be a mixture with graphite, boron and nitrogen. By a similar procedure, Suenaga et al,[9] produced B-C-N nanotubes with well-separated layers of BN and carbon. Redlich et al,[10] synthesized B-C-N nanotubes having a BC_2N outer shell and a carbon inner shell by the arc-discharge method. Nanotubes of outer BC_7N layers and pure carbon inner layers have been obtained by laser ablation using a composite of BN and carbon as the target in the presence of nickel and cobalt.[11] Rao et al,[12] prepared B-C-N nanotubes of varying compositions of carbon and nitrogen by the pyrolysis of BH_3-trimethylamine adduct. A template based approach has also been reported to prepare B-C-N nanotubes using graphitic carbon nanotubes and carbon nitride nanotubes.[13,14] BC_4N powder has been obtained by the nitridation of boric acid and carbonization of saccharose in molten urea.[15] Single walled carbon nanotubes doped with B and N have also been prepared by a hot filament

method.[16] Multiwalled nanotubes of the composition B_5CN_5 have been produced by chemical vapor deposition along with nanotubes containing BN layers sheathed with outer carbon layers.[17] While the arc-discharge and laser ablation methods have drawbacks in controlling phase separation and the diameter of the nanotubes, the template based method has the limitation in extending the diameter of the B-C-N nanotubes beyond 20 nm. Furthermore, the surface of pristine carbon nanotubes is generally not reactive. In the present study, we have employed amorphous carbon nanotube (a-CNT) brushes[18] prepared by the decomposition of glucose as starting materials to prepare the BCN nanotube brushes. We have introduced BN in a-CNTs by using the boric acid-urea mixture. Interestingly, the nanotubes obtained by us have the composition BC_4N and are nonmagnetic insulators. To our knowledge, BC_4N nanotubes have not been investigated hitherto.

3.3 Experimental and related aspects

Synthesis

Amorphous carbon nanotubes

Amorphous carbon nanotube (a-CNT) brushes were prepared by the following procedure. Polycarbonate membranes with a pore diameter of 220 nm were soaked in 22 mL of 0.5 M aqueous solution of glucose in a 25 mL Teflon-lined autoclave. The same procedure

was repeated with polycarbonate membranes with a pore diameter of 50 nm. The temperature of the autoclave was maintained at 180 °C for 6 h after which it was allowed to cool to room temperature. The brownish liquid, rich in carbon spheres was discarded. The membranes that had turned brown were washed with deionized water and ethanol several times and dried at 40 °C for 1 h.

BC_4N nanotube brushes

A mixture of boric acid (1g) and urea (11.8 g) was taken in 40 ml distilled water and heated at 70 °C until the solution became viscous; the a-CNTs were soaked in it for nearly 2 h. They were later separated physically and dried in air at 40 °C for overnight. The dried sample was thermally treated at 970 °C for 3 h for 40 nm nanotubes in a N_2 atmosphere, and for 12 h in the case of the larger diameter (170 nm) nanotubes, and then cooled down to room temperature. The product was subsequently heated in NH_3 atmosphere at 1050 °C in case of 170 nm nanotubes and 900 °C in case of 40 nm nanotubes for three hours to give black-coloured boron-carbon-nitride nanotube brushes. The products were investigated by transmission electron microscopy and other physical techniques.

Nanoparticles coating

In order to obtain Au/Pt nanoparticles-covered BCN nanotube brushes, the nanotubes obtained by the template method described earlier, were soaked in 2 mL of 5 mM aqueous solutions of hydrogen

hexachloroplatinate (IV) or hydrogen tetrachloroaurate (III) for 12 h. The nanotubes were washed twice with distilled water followed by a washing with 10 mM sodium borohydride solution before drying at 40 °C for an hour. The resulting products were examined by electron microscopy.

Techniques used for characterization

X-ray diffraction (XRD): XRD patterns of the nanotubes were recorded at 25 °C with a Rich-Siefert 3000-TT diffractometer employing Cu Kα radiation.

Scanning Electron Microscope: The morphology of the nanotubes was examined by a Field Emission Scanning Electron Microscope (FESEM, FEI Nova-Nano SEM-600, Netherlands), and scanning electron microscope (SEM) Leica S-440I instrument (U.K).

Transmission Electron Microscope: TEM images were recorded with a JEOL JEM 3010 instrument (Japan) operated at an accelerating voltage of 300 kV.

X-ray Photoelectron Spectroscopy (XPS): X-ray photoelectron spectroscopy measurements were performed using ESCALAB MKIV spectrometer employing Al Kα radiation (1486.6 eV).

Electron Energy Loss Spectra (EELS): Electron energy loss spectra (EELS) were recorded with a transmission electron microscope (FEI,

TECNAI F30) equipped with an energy filter for (EELS) operating at 300 kV.

Raman spectra: Raman spectra were recorded with a LabRAM HR with 633 nm line from HeNe laser.

Thermogravimetric analysis: Thermogravimetric analysis was carried out using a Mettler Toledo Star system.

Gas adsorption: Nitrogen adsorption-desorption isotherms were measured at liquid N_2 temperature (77 K) using QUANTACHROME AUTOSORB-1C surface area analyzer. The surface area was obtained by using the BET method. The CO_2 adsorption was carried out at 195 K (1:1 mixture of dry ice and acetone). Hydrogen adsorption was carried out at liquid nitrogen temperature (77.36 K).

Magnetization measurements: Magnetization measurements were carried out with a vibrating sample magnetometer in a physical property measuring system (PPMS,Quantum Design, San Diego, CA, USA).

3.4 Results and Discussion

Characterization of nanotube brushes

Figure 1a shows a FESEM image of the amorphous carbon nanotubes (a-CNT) with well-aligned brush-like morphology. The TEM image in Figure 1b shows the outer diameter of the a-CNT to be around 250 nm with a wall thickness of about 50 nm.

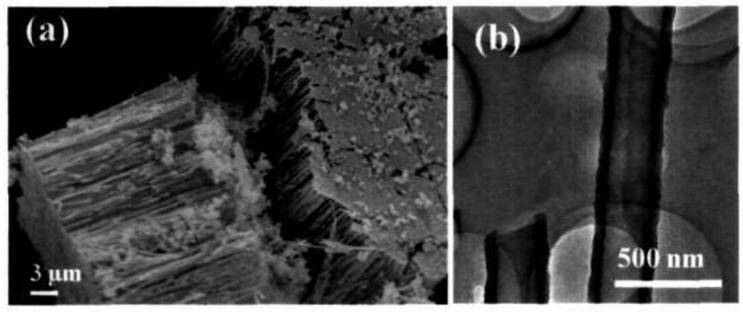

Figure 1: (a) SEM Image of amorphous carbon nanotube brushes. (b) TEM Image of individual amorphous carbon nanotubes

After the reaction of a-CNT brushes with the H_3BO_3–urea mixture, we obtain the nanotube structures shown in Figure 2a. These structures containing B, C and N replicate the brush-like morphology of the a-CNTs. The diameter of the BCN nanotubes is 170 nm and the lengths are 15 μm. The higher magnification FESEM image in Figure 2b shows the open ends of the BCN nanotubes demonstrating the wall thickness to be around 50 nm. This is further supported by the TEM image of a single nanotube shown in Figure

2c. The selected area electron diffraction pattern shows faint rings, with a few spots. The XRD pattern of the BCN nanotube brushes (Figure 3a) shows broad reflections with d spacing's 3.43 Å and 2.13 Å corresponding to (002) and (100) planes respectively. This pattern is similar to that reported for BC_3N, (JCPDS card: No. 35-1292). The broad reflections in the XRD pattern and the diffused rings in electron diffraction pattern suggest the turbo static nature of the nanotubes as reported earlier for the other preparations of BCN

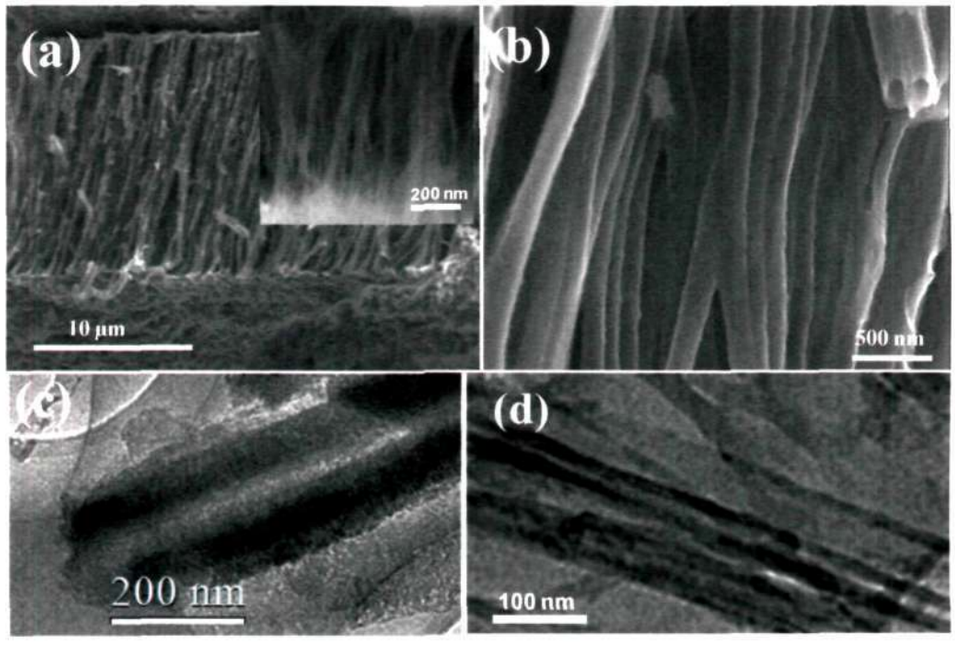

Figure 2: (a) FESEM images of BC_4N nanotube brush with an average diameter of a single tube around 170 nm. Inset shows a FESEM image of BC_4N nanotube brushes of diameter 40 nm. (b) Higher magnification FESEM images of BC_4N nanotube brushes. TEM image of a BC_4N nanotube c) 170 nm diameter. (d) 40 nm diameter

materials.[1] We have prepared a-CNTs using a polycarbonate membrane with a pore size of 50 nm. Using the a-CNTs, we have

obtained BC_4N nanotube brushes. FESEM image of the BC_4N nanotube brushes of diameter 40 nm is shown in the inset of Figure 2a. TEM images of the BC_4N nanotubes of diameter 170 and 40 nm are shown in Figure 2c and 2d respectively.

The Raman spectra of the BC_4N nanotubes were recorded with the 633 nm line from a HeNe laser. The spectra are shown in Figure 3b. The observation of two strong peaks at 1324 cm^{-1} and at 1600 cm^{-1} in the Raman spectra are the signatures of D band and G bands of BCN nanotubes.[19,20] The D bands are somewhat broad probably due to the disorder in the BCN layers. The additional peak at around 800 cm^{-1} is similar to that found in BN nanotubes. The band around 2600 cm^{-1} may be due to combination D + G band or 2D overtone. Such bands have been observed in BCN nanotubes of other compositions.[19,20]

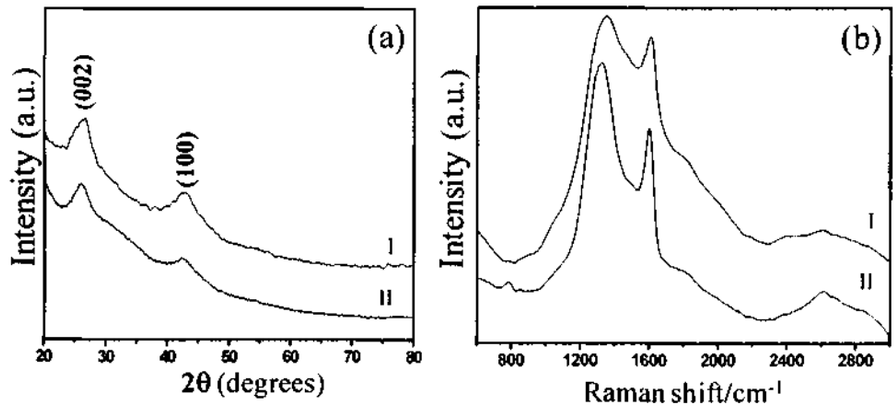

Figure 3: (a) XRD (b) Raman spectrum of BCN nanotube brushes. (I) 40 nm diameter (II) 170nm diameter.

X- ray Photoelectron spectra of the BCN nanotubes in the N, C and B (1s) regions are shown in Figure 4. We can analyze these data on the lines suggested by Kim et. al.[17] The N 1s spectrum of the BCN nanotube brushes in Figure 4a shows peaks at 397.7 eV, 400.2 eV and 401.5 eV. The peak at 397.7 eV corresponds to nitrogen bonded to boron (N–B bond), peak at 400.2 eV corresponds to nitrogen bonded with carbon in graphite like N–C structure, and the peak at 401.5 eV assigned to N bonded to C in a pyridine type structure. The C 1s spectrum in Figure 4b has two peaks with a broad shoulder. The peak at 284 eV is assigned to carbon bonded

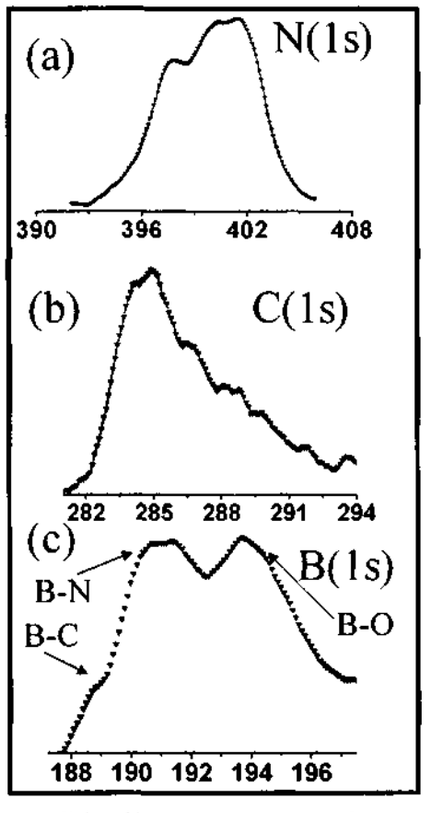

Figure 4: XPS taken on the surface of the BCN nanotube brushes

with boron atoms (C-B bond) and the peak at 286 eV corresponding to a carbon bonded to another carbon atom (C-C bond). The long tapering band extending from 286 eV to 289 eV is ascribed to carbon atoms bonded to nitrogen. The B 1s spectrum in Figure 4c has two peaks centered at 191.2 eV and 194 eV, with a shoulder at 189.2 eV. The shoulder at 189.2 eV corresponds to boron bonded to carbon (B-C bond), and the peak at 191.2 eV is due to boron bonded to nitrogen (B-N bond). The peak at 194 eV is assigned to boron bonded to oxygen (B-O bond), probably arising from the excess B_2O_3. By subtracting the contribution of the B-O part from the B 1s signal, we have estimated the composition of the nanotubes taking the capture cross sections into account. Such an analysis gave the approximate composition of the BCN nanotube brushes to be $BC_4N_{1.5}$.

In order to obtain a more reliable elemental analysis, we carried out electron energy loss spectroscopy (EELS) measurements on the K-edge absorption for B, C, and N in a high-resolution electron microscope. The spectrum clearly shows K-shell ionization edges at 188, 284, and 401 eV for B, C and N respectively. Each core edge fine structure consists of a sharp π^* peak and a well-resolved σ^* band, characteristic of sp^2 hybridization.[21] The percentage of B and N were significantly smaller than that of carbon. EELS measurements gave an average chemical composition, BC_4N for these nanotubes. In Figure 5 we show the elemental mapping of the nanotubes the red, green and blue colours representing boron, carbon and nitrogen

respectively. We see that the colours are randomly distributed across the nanotubes suggesting that the nanotubes are homogeneous with a uniform distribution of B, C and N atoms. The homogeneous nature of the BC_4N nanotubes is also confirmed by the fact that we failed to obtain BN nanostructures after removal of carbon from the BC_4N nanotubes by oxidation.[22]

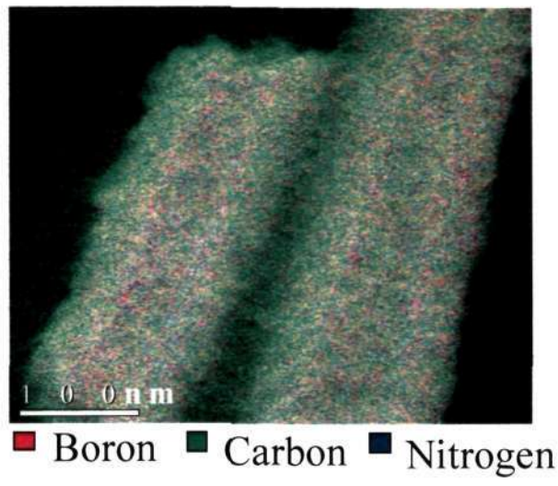

Figure 5: Elemental mapping of Boron, Carbon and Nitrogen of BCN nanotubes obtained from EELS

Properties of BC_4N nanotube brushes

We have carried out thermogravimetric analysis of BC_4N nanotubes in air. These nanotubes show high thermal stability and no weight loss was observed up to 900 °C (Figure 6). Amorphous carbon nanotubes get completely oxidized before 750 °C. The high thermal stability of BC_4N nanotubes is noteworthy.

In the literature, there have been theoretical papers describing magnetism of BCN nanotubes. BCN nanotubes having an approximate composition of BC_2N have been predicted to be ferromagnetic.[23] Such itinerant ferromagnetism has also been predicted in C-BN heterostructured nanotubes.[24] BCN ribbons of the composition $BC_{10}N$ have been predicted to be ferrimagnetic.[25] Carbon doping in BN nanotube is supposed to induce spontaneous

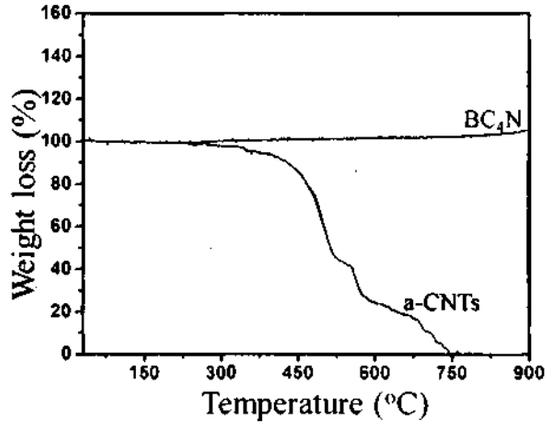

Figure 6: TGA of (I) BCN nanotubes (II) a-CNT

magnetism.[26] The magnetic susceptibility measurement on BC_4N nanotube brushes shows that they are nonmagnetic. They show a very small magnetic moment (0.22 μ_B) probably due to defect in the nanotubes. The BC_4N nanotubes are highly insulating, the resistivity being in the mega-ohm region.

Adsorption properties of materials are of importance in gas storage, selective gas recognition and separation. Zeolites and metal-organic frameworks have enjoyed high utility in gas adsorption

because of the high surface area, and well defined pore shapes. We have measured the surface area of the as synthesized BC_4N nanotube brushes using nitrogen adsorption-desorption isotherms performed at 77 K (Figure 7a). The surface area measured by Brunauer, Emmett and Teller (BET) method was 356 m^2/g with contributions from micropores (0.7 nm) and mesopores (4 nm) as can be seen from the inset in Figure 7a. The CO_2 adsorption on the BC_4N nanotube

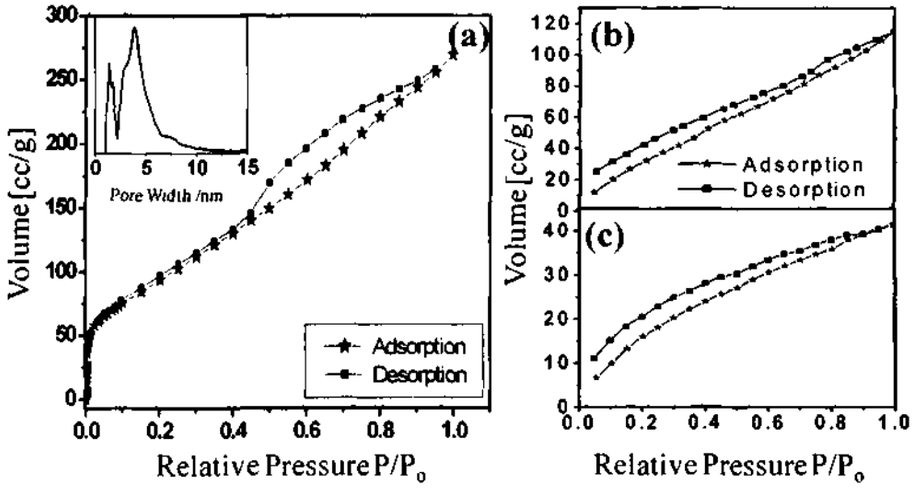

Figure 7: Adsorption - desorption isotherm of (a) N_2 at 77 K (Inset shows the pore size distribution) (b) CO_2 at 195 K and (c) H_2 at 77 K of BCN nanotube brushes

brushes was measured at low pressures and low temperature at 195 K. The BC_4N nanotube brushes showed remarkably high CO_2 uptake of about 23.5 wt % (Figure 7b). The adsorption does not exhibit saturation even at $P/P_o = 1$, indicating the presence of unoccupied pores available for further uptake. The adsorption of hydrogen on the BC_4N nanotubes was only 0.4 wt % at 77 K (Figure 7c). Thus, the

BC_4N nanotubes prepared by us are selective adsorbents of CO_2. New materials having selective adsorption for CO_2 are important for environment and industrial applications. Millward and Yaghi[27] have studied CO_2 adsorption by various metal-organic frameworks (MOF), and reported the highest value of adsorption (33.5 mmol/g) in the case of MOF-177 at ambient temperature and high pressures. Among the zeolites, the highest reported value of CO_2 adsorption is 7.4 mmol/g for Zeolite 13X at high pressures and room temperature.[28] Sudik et al,[29] measured CO_2 adsorption at 195 K and low pressures in certain iron carboxylate MOFs and reported highest CO_2 uptake for IRMOP-51 of 74 $cm^3(STP)/cm^3$.

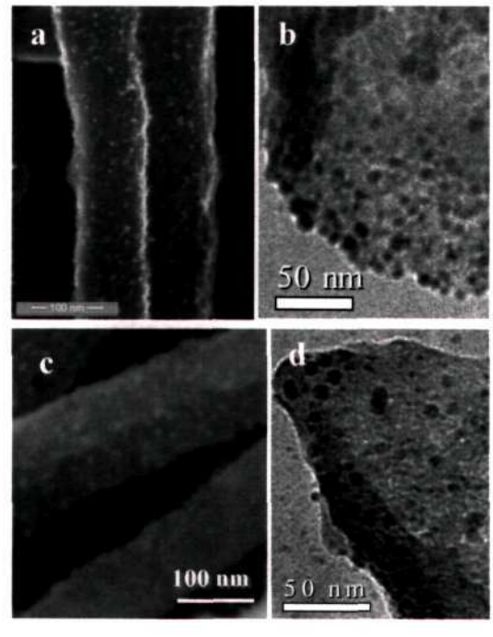

Figure 8: (a) FESEM image b) TEM image of Pt decorated BCN nanotubes. (c) FESEM image d) TEM image of Au decorated BCN nanotubes.

In Figure 8, we show the FESEM images of BC_4N nanotubes decorated with Pt and Au nanoparticles. We see a uniform distribution of nearly monodispersed metal nanoparticles on the nanotube walls. The size of the metal nanoparticles is in the range of 3-8 nm as found from the TEM images in Figure 8b and 8d. Such metal nanoparticle decorated BC_4N nanotubes could have useful applications.

Thanks to Prof. U. V. Waghmare, Prof. Swapan. K. Pati and Dr. Mousumi Upadhyay-Kahaly for carrying out first-principles density functional theory based calculations to understand the structure and properties of BC_4N nanotubes. The most stable structure is predicted to be the one where BN_3 and NB_3 units connected by a B–N bond are present in the graphite matrix. The other structure with a slightly higher energy is the one with ordered B–N bonds in all the six-membered rings. The latter structure is chemically more sensible. Calculations on (6,0), (6,6) and (8,0) BC_4N naotubes show that they all are nonmagnetic and both (6,0) and (6,6) BC_4N nanotubes open up a small semiconducting gap along with the (8,0) BC_4N nanotube.

3.5 Conclusions

It has been possible to synthesize nanotubes of the composition BC_4N starting with a-CNTs prepared with the porous polycarbonate membranes. The reaction of the a-CNTs with a mixture of urea and boric acid provides an excellent means for the incorporation of boron and nitrogen in the carbon nanotubes. In the first step of the reaction, the decomposition of urea produces NH_3, which on reaction with boric acid at high temperatures enables the incorporation of both boron and nitrogen in the carbon nanotubes. The BC_4N nanotubes have been characterized by various physical methods and the composition established by EELS carried out in a high-resolution electron microscope. Although the nanotubes may not have an extended ordered structure with graphitic type BCN layers, there exists a sufficient order to give X-ray diffraction patterns and well-defined Raman spectra. Surprisingly, BC_4N nanotubes have very high thermal stability. They are nonmagnetic insulators with a high propensity for CO_2 uptake (up to 23.5 wt %).

References

1. M. Kawaguchi, *Adv. Mater.*, **9**, *8*, 1997.

2. C. Y. Zhi, X. D. Bai, and E. G. Wang, *J. Nanosci. Nanotech.*, **4**, *35*, 2004.

3. X. D. Bai, E. G. Wang, J. Yu and H. Yong, *Appl. Phys. Lett.*, **77**, *67*, 2000.

4. J. Yu, J. Ahn, S. F. Yoon, Q. Zhang, Rusil, B. Gan, K. Chew, M. B. Yu, X. B. Bai and E. G. Wang, *Appl. Phys. Lett.*, **77**, *1949*, 2000.

5. J. Yu, X. D. Bai, J. Ahn, S. F. Yoon and E. G. Wang, *Chem. Phys. Lett.*, **323**, *529*, 2000.

6. R. B. Kaner, J. Kouvetakis, C. E. Warble, M. L. Sattler and N. Bartlett, *Mater. Res. Bull.*, **22,** *399*, 1987.

7. Nanotubes and Nanowires, C. N. R. Rao, A Govindaraj, RSC Publishing, Cambridge, 2005.

8. O. Stephan, Ajayan, P. M. Colliex, C. Redlich, Ph. Lambert, J. M. Bernier and P. Lefin, *Science*, **266**, *1683*, 1994.

9. K. Suenaga, C. Colliex, N. Demoncy, A. Loiseau, H. Pascard and F. Willaime, *Science*, **278**, *653*, 1997.

10. Ph. Redlich, J. Loeffler, P. M. Ajayan, J. Bill, F. Aldinger and M. Riihle, *Chem. Phys. Lett.*, **260,** *465*, 1996.

11. Y. Zhang, H. Gu, K. Suenaga and S lijirna, *Chem. Phys. Lett.*, **279,** *264,* 1997.

12. R. Sen, B. C. Satishkumar, A. Govindaraj, K. R. Harikumar, G. Raina, J. P. Zhang, A. K. Cheetham and C. N. R. Rao, *Chem. Phys. Lett.*, **287**, *671,* 1998.

13. W. Q. Han, J. Cumings, X. Huang, K. Bradley and A. Zettl, *Chem. Phys. Lett.*, **346,** *368,* 2001.

14. M. Terrones, D. Golberg, N. Grobert, T. Seeser, M. R. Reyes, M. Mayne, R. kamalakaran, P. Dorozhkin, Z. C. Dong, H. Terrones, M. Ruhle, and Y. Bando, *Adv. Mater.*, **15**, *1899*, 2003.

15. M. Hubacek, and T. Sato, *J. Solid State Chem.*, **114**, *258*, 1995.

16. W. L. Wang, X. D. Bai, K. H. Liu, Z. Xu, D. Golberg, Y. Bando, and E. G. Wang, *J. Am. Chem. Soc.*, **128,** *6530,* 2006.

17. S. Y. Kim, J. Park, H. C. Choi, J. P. Ahn, J. Q. Hou, and H. S. Kang, *J. Am. Chem. Soc.*, **129,** *1705*, 2007.

18. J. Dinesh, M.Eswaramoorthy and C. N. R. Rao, *J. Phys. Chem. C,* **111,** *510,* 2007.

19. C. Y. Zhi. X. D. Bai, and E. G. Wang, *Appl. Phys. Lett.*, **80,** *3590,* 2002.

20. J Wu, W. Q. Han, W. Walukiewicz, J. W. Ager and W shan, *Nano. Lett.*, **4,** *647*, 2004.

21. X. D. Bai, C. Y. Zhi, and E. G. Wang, *J. Nanosci. Nanotech.*, 2001, 1, 55.

22. W. Q. Han, W. Mickelson, J. Cumings and A. Zettl, *Appl. Phys. Lett.*, **81,** *1100*, 2002.

23. S. Okada, and A. Oshiyama, *Phys. Rev. Lett.*, **84,** *146803*, 2001.

24. J. Choi, Y. H. Kim, K. J. Chang, and D. Tomanek, *Phys. Rev. Lett.*, **67**, *14680*, 32003.

25. J. Nakamura, T. Nitta and A. Natori, *Phys. Rev. Lett.*, **72**, *205429*, 2005.

26. R. Q. Wu, L. Liu, G. W. Peng, and Y. P. Feng, *Appl. Phys. Lett.*, **86,** *122510*, 2005.

27. A. R. Milliward and O. M. Yaghi, *J. Am. Chem. Soc.*, **127,** *17998*, 2005.

28. S. Cavenati, C. A. Grande and A. E. Rodrigues, *J. Chem. Eng. Data,* **49,** *1095*, 2004.

29. A. C. Sudik, A. R. Millward, N. W. Ockwig, A. P. Cote, J. Kim and M. Yaghi, *J. Am. Chem. Soc.*, **127,** *7110*, 2005.

CHAPTER 4

A study of the transformations of elemental nanowires to nanotubes of metal oxides and chalcogenides through Kirkendall effect

Summary

This chapter of the thesis deals with the transformations of elemental nanowires of metals and silicon to nanotubes of the corresponding oxides and chalcogenides through Kirkendall effect. The metal nanowires were prepared by nebulized spray pyrolysis of metal acetates in an inert atmosphere and silicon nanowires by carbon-assisted synthesis. The formation of ZnO nanotubes by the oxidation of Zn nanowires has been studied as a function of time observing the intermediate structures during the oxidation. Nucleation of Kirkendall voids in the nanowires during the oxidation leads to the formation of the ZnO nanotubes. The kinetics of the Zn nanowire-ZnO nanotube

---

Paper based on this work has been submitted to J. Phys. Chem. C (2008)

transformation has been studied and the activation energy for the transformation found to be 12.2 kcal/mol. $ZnCr_2O_4$ nanotubes are formed by the reaction of Zn nanowires with CrO_2Cl_2 in an oxygen atmosphere. We have obtained nanotubes of Co_3O_4, starting from Co nanowires and SiO_2 (cristobalite) nanotubes starting from Si nanowires. Nanotubes of ZnS, CdS and CdSe have been obtained by the reaction of the metal nanowires with the chalcogens. The activation energy for the formation of CdS nanotubes from Cd nanowires is found to be 8.5 kcal/mol. The present study establishes Kirkendall effect as a novel means of preparing nanotube structures of several inorganic materials.

4.1 Introduction

Kirkendall effect involves a non-equilibrium mutual diffusion process of a diffusion couple through the interface such a directional flow of atoms is balanced by the flow of vacancies.[1] When the nanostructure of a fast-diffusing species reacts with a slower-diffusing species, a large number of vacancies are created because of the high surface to volume ratio of the nanostructure as well as the absence of defects at the core. Inside the small volume of the growing nanostructure the vacancies coalesce into large voids giving rise to products which are hollow nanostructures. Synthesis of hollow nanostructures employing the Kirkendall effect would have several advantages.[2]

Kirkendall effect was established by E. O. Kirkendall in 1947 in the case of a diffusion couple consist of copper and brass.[1,3] He has shown that the intrinsic diffusivity of Zn is ≈ 2.5 times that of Cu at 785 °C. Kirkendall effect was considered as a destructive effect because formation of Kirkendall voids deteriorates the bonding strength of bond-pad interface or may cause wire bond failure in integrated circuits.[4,5] Engineers try to avoid this effect by introducing diffusion barrier layers, for example Ta as a diffusion barrier between Cu and bronze in the multifilamentary superconducting composite.[6] After more than sixty years Kirkendall effect has received scientific attention once again when

chemists have used this destructive effect in a constructive way for the fabrication of hollow nanostructures.

4.2 Scope of the present study

Nanotubes are nanomaterials of great importance due to their novel properties and potential applications in diverse areas as high-efficiency catalysts, drug delivery systems, nanoelectronics, nano-optics, light weight structural materials and energy storage and conversion.[7,8] Compared to nanowires, nanotubes provide access to three different contact regions: the inner surface, the outer surface and the tube ends. Several methods of synthesizing carbon as well as inorganic nanotubes have been described in the literature.[7,8] Typical of the synthetic methods are template-assisted growth, arc discharge, laser ablation, chemical vapour deposition, plasma enhanced vaporization and hydrothermal or solvothermal processes. Hollow nanostructures can also be created by making use of the Kirkendall effect. Hollow spherical nanostructures of cobalt oxides, sulphides and selenides have been obtained by making use of the Kirkendall effect.[9] Nanotubes of Ag_2Se have been prepared by UV photodissociation of CSe_2 adsorbed on the surface of Ag nanowires.[10] While Ga doped ZnS nanowires have been converted in to $ZnO\text{-}ZnGa_2O_4$ composite nanotubes,[11] $ZnAl_2O_4$ nanotubes were obtained by the interfacial solid state reaction of core-shell $ZnO\text{-}Al_2O_3$ nanowires.[12] Formation of Co_3S_4 nanotubes starting from 1D

$Co(CO_3)_{0.35}Cl_{0.20}(OH)_{1.10}$ nanowires appears to involve Kirkendall effect.[13] In spite of these literature reports, there is no detailed investigation of the structures as well as the formation kinetics of 1D hollow nanostructure of oxides and other materials formed by the transformations of metallic or elemental nanowires through Kirkendall effect. We have, therefore, carried out a systematic study of the formation of ZnO nanotubes from Zn nanowires by employing X-ray diffraction and electron microscopy, paying attention to the process of transformation. $ZnCr_2O_4$ nanotubes have been formed by the reaction of Zn nanowires with CrO_2Cl_2. We have obtained nanotubes of Co_3O_4, ZnS, CdS and CdSe starting with the corresponding metallic nanowires, besides SiO_2 (cristobalite) nanotubes starting from Si nanowires. Kinetics of formation of the CdS nanotubes from Cd nanowires has also been examined.

4.3 Experimental and related aspects

Synthesis

Metal nanowires

Nanowires of Zn, Co and Cd were synthesized by the nebulised spray pyrolysis of methanolic solutions of the metal acetates in an inert atmosphere.[14] In a typical experiment, 50 ml methanolic solution of acetate of zinc, cadmium or cobalt was prepared with a concentration of 40 gL^{-1}. The solution was nebulized and the spray carried into a preheated silicon carbide furnace maintained between 820 and 850 °C using Ar as a carrier gas. Typical flow rates of Ar used was 1000 standared cubic centimetre per minute (sccm). All the experiments were performed using a quartz tube with an inner diameter of 25 mm. The reaction was typically carried out for 1 h. The shiny deposits obtained at the outlet of quartz tube was characterized to be metal nanowires and used for the further experiments.

Silicon nanowires

Si nanowires were obtained by heating an intimate mixture of silicon powder and activated charcoal in nitrogen environment.[15] In typical experiment silicon powder was finely ground with activated charcoal keeping the weight ratio of Si to C at 1:3 and the mixture was heated at 1200 °C for 3 h in an N_2 atmosphere. The grey colour powder obtained

as the final product was identified as Si nanowires and used for further experiments.

Oxides nanotubes

The Zn nanowires were heated at around 430 °C for 4 h in air to transform them to ZnO nanotubes. The progress of the reaction was followed by recording electron microscopy images as well as X-ray diffraction patterns at intermediate stages of the transformation. The kinetic data were obtained by recording X-ray diffraction patterns at different stages of the conversion in the 380-430 °C range. We have carried out the reaction of Zn nanowires with CrO_2Cl_2 at 400 °C for 3h to obtain $ZnCr_2O_4$ nanotubes. CrO_2Cl_2 was produced in a gas trap by adding a mixture of KCl and $K_2Cr_2O_7$ to concentrated H_2SO_4. In a typical experiment, a mixture of 1 g KCl and 1 g $K_2Cr_2O_7$ was added to 25 mL of conc H_2SO_4. Oxygen gas was passed through the trap to carry the CrO_2Cl_2 vapour towards the Zn nanowires placed in a tube furnace. In order to prepare Co_3O_4 nanotubes, Co nanowires were heated in air at 500 °C for 5 h. The intermediate structures during Co_3O_4 nanotubes formation was examined at 450 °C/5 h. To prepare SiO_2 nanotubes, oxidation of Si nanowires was carried out at 1325 °C for 5 h in air.

Chalcogenides nanotubes

Zn nanowires (30 mg) were mixed thoroughly with sulphur powder (150 mg) and the mixture was heated in an Ar atmosphere at 500 °C for 3 h to obtain ZnS nanotubes. CdS nanotubes were synthesised by heating a finely ground mixture of Cd nanowires and sulphur powder (1:9 molar ratio) at 500 °C for 3 h in an Ar atmosphere. The kinetics of the reaction was studied by recording XRD patterns at different time intervals. CdSe nanotubes were obtained by heating a mixture of Cd nanowires and selenium powder (1:5 molar ratio) at 400 °C for 3 h in an Ar atmosphere.

Techniques used for characterization

X-Ray diffraction (XRD): XRD patterns were recorded at 25 °C with a Rich-Siefert 3000-TT diffractometer employing Cu Kα radiation.

Electron Microscopy: Field emission scanning electron microscopy (FESEM) and scanning tunnelling electron microscopy (STEM) images were recorded with a field emission scanning electron microscope (FESEM, FEI Nova-Nano SEM-600, Netherlands). TEM images were recorded with a JEOL JEM 3010 instrument (Japan) operated at an accelerating voltage of 300 kV.

4.4 Results and discussion

Zn nanowires

In Figure 1a, we show a low-magnification FESEM image of Zn nanowires obtained by nebulized spray pyrolysis of a methanolic solution of zinc acetate. The nanowires have lengths of several tens of

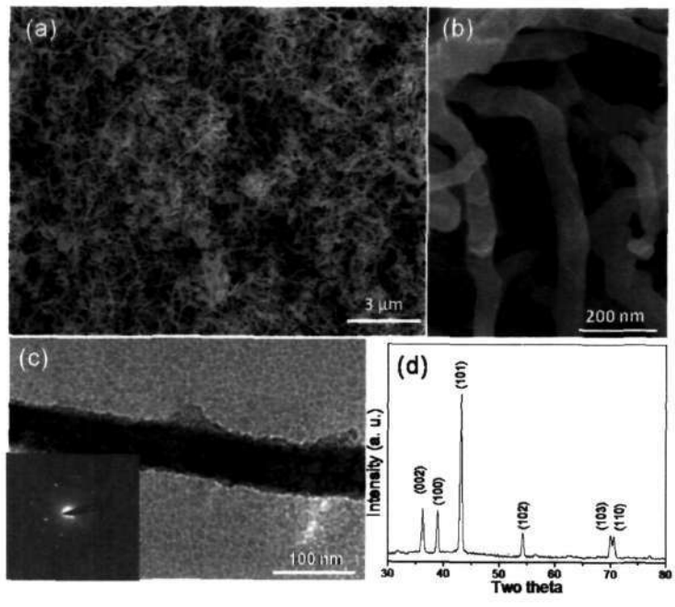

Figure 1. (a) Low-magnification and (b) higher-magnification FESEM images of Zn nanowires, (c) TEM image of a Zn nanowire (the inset is the SAED pattern), (d) XRD pattern of Zn nanowires.

micrometers with zigzag morphology. The higher magnification FESEM image in Figure 1b, shows the nanowires to have a smooth surface with an average diameter 50 nm. The TEM image in Figure 1c, along with the selected area electron diffraction (SAED) pattern shown as an inset,

confirms the nanowires to be single crystalline. The X-ray diffraction (XRD) pattern (Figure 1d) is characteristic of the hexagonal structure of zinc (JCPDS card: No. 04-0831, a = 2.67 Å and b = 4.95 Å).

ZnO nanotubes

Thermal oxidation of Zn nanowires in air in the temperature range 653 - 703 K for 2 – 4 hours was found to yield ZnO nanotubes. The tubular structure of ZnO nanotubes is clearly seen in the FESEM image (Figure 2a). The outer diameters of the nanotubes go up to 90 nm with

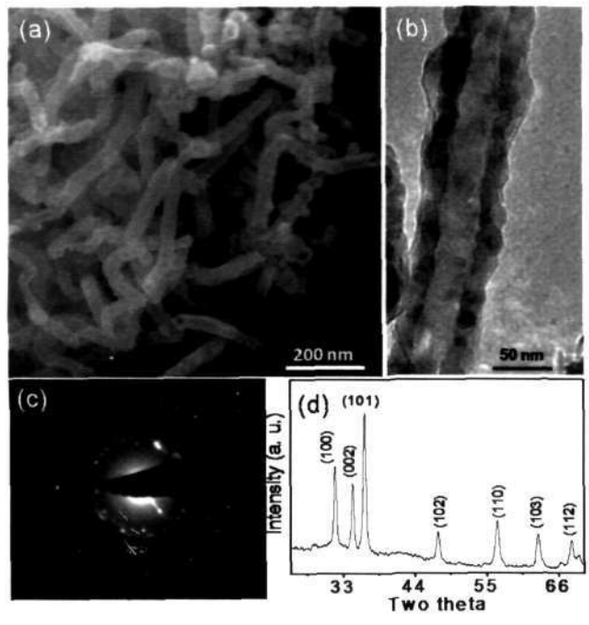

Figure 2. (a) FESEM image of ZnO nanotubes, (b) TEM image of a ZnO nanotube, (c) SAED pattern of ZnO nanotube, (d) XRD pattern of ZnO nanotubes.

lengths varying from 400 nm to few microns. The TEM image of a ZnO nanotube shown in Figure 2b demonstrates the wall thickness to be

around 20 nm. Thus, the inner diameter of the nanotubes works out to be close to the diameter of the starting metal nanowires. The SAED pattern of the ZnO nanotube (Figure 2c) shows some ring patterns, but with prominent Bragg spots. The XRD pattern shown in Figure 2d could be indexed for the hexagonal unit cell of ZnO (JCPDS card: No. 36-14151, $P6_3mc$, a = 5.25 Å and c = 5.21 Å).

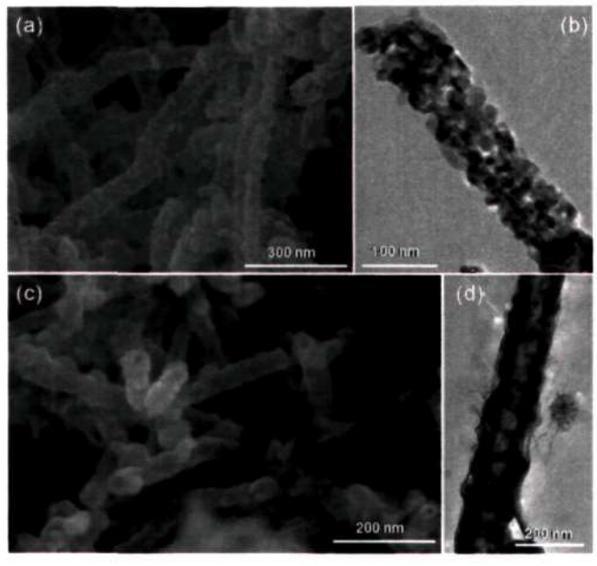

Figure 3. (a) FESEM image and (b) TEM image of the nanostructure obtained after oxidation for 15 min, (c) FESEM image and (d) TEM image obtained after 1 h of oxidation.

The formation of ZnO nanotubes by the oxidation of Zn nanowires was studied as a function of time, observing the intermediate structures during the oxidation of the metal nanowires. A FESEM image of Zn nanowires after oxidation for 15 min is shown in Figure 3a. We see the

rough surface of the 1D nanostructure compared to the initial smooth surface of Zn nanowires. A TEM image in Figure 3b reveals the porous nature of nanostructure. After oxidation for one hour, the surface roughness of the nanostructure decreases and openings of tube-like structures begin to appear as can be seen from the FESEM image in Figure 3c. The pores formed after oxidation for 15 minutes coalesce to form bigger pores resulting a bamboo type nanotube structure after 1 h as shown in the TEM image in Figure 3d. After the oxidation was carried out for 4 h, well-defined nanotubes of ZnO are formed as shown in Figure 2.

The porous nature of the intermediate nanostructures and the polycrystalline nature of the product nanotubes suggest that the conversion of Zn nanowires into ZnO nanotubes involves nano-scale Kirkendall effect.[8-13,16] The faster outer diffusion of zinc atoms compared to the slower inner diffusion of the oxygen atoms through the initially formed ZnO layer is compensated by the opposite flow of vacancies, the vacancies coalescing together to form larger Kirkendall voids. The Kirkendall voids condense into form the bigger holes in the nanostructures, giving rise to bamboo-like morphology. After this stage, it takes another 2 to 3 h to form perfect tubular nanostructures since the increasing thickness of the ZnO layer does not favour the outer diffusion of Zn atoms.

The kinetics of formation ZnO nanotubes was studied by recording XRD patterns at different time intervals at 653, 673 683 and 703 K. The reflections correspond to both Zn and ZnO coexist in all the patterns shown in Figure 4, but the reflections corresponding to ZnO increase in intensity with time, accompanied by a decrease in the intensity of the

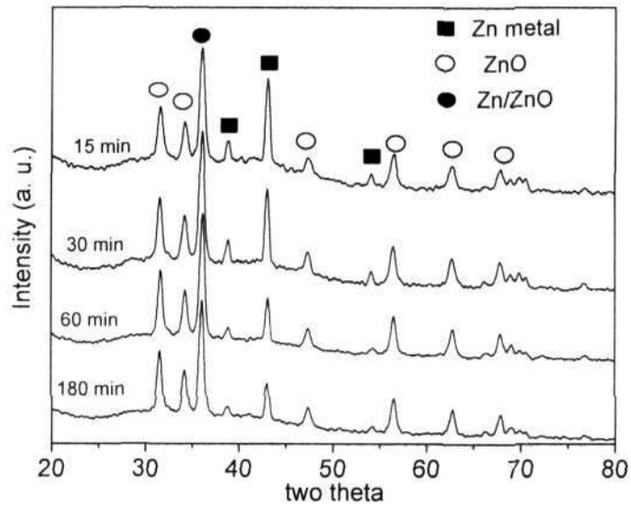

Figure 4. XRD patterns recorded at different time intervals of the Zn nanowires-ZnO nanotubes transformation.

reflections due to Zn metal. We have determined the areas under the (100) reflection of ZnO and the (101) reflection of Zn and plotted the ZnO:Zn ratio of areas against the reaction time in Figure 5a (open symbols) at different temperatures. These experimental data could be fitted to the logarithimic rate law.

$$y = k \log (a\ t + 1) + b \qquad (1)$$

where t is time in minutes, k is the rate constant, a and b are temperature-dependant constants and y is the ZnO/Zn ratio. The logarithmic rate law is widely used to explain the oxidation of metals,[17-22] arises from the mechanism proposed by Caberra and Mott, Grimley

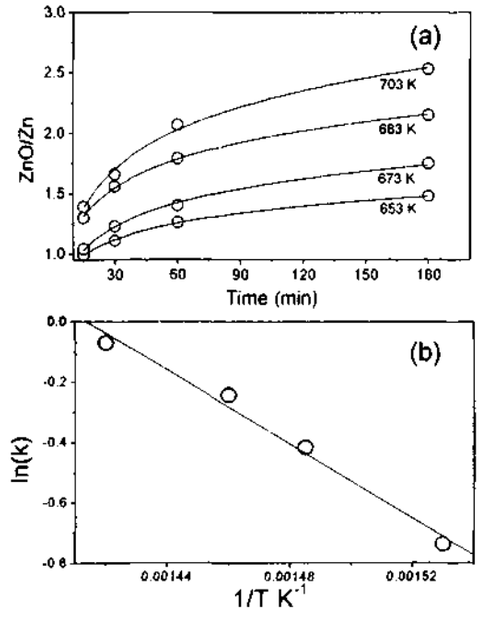

Figure 5. (a) Plots of the ratios of areas under ZnO (100) and Zn (101) reflactions against reaction time at different temperatures (open symbols). Solid curves represent the logarithimic rate law fit to the experimental data. (b) Arrhenius plot of lnk against 1/T.

and Trapwell, and Eley and Wilkinson, where either cation or anion diffusion limits the rate of oxide growth.[20-24] There is an initial period of rapid oxidation followed by a virtual cessation of the reaction and the formation of a stable film, a few nanometers in thickness. The goodness

of the fits of the experimental data to Equation (1) can be seen by the solid curves shown in Figure 5a. From these data we have derived the value of k in Equation (1). A plot of lnk against inverse of absolute temperature is given in Figure 5b. This plot yields an activation energy for the nanotubes formation of 12.2 kcal/mol. The activation energy for the oxidation of bulk Zn is repoted to be 28.1 kcal/mol.[25,26] Thus, the activation energy for the oxidation by Kirkendall effect involving diffusion processes is associated with a lower activation energy.

$ZnCr_2O_4$ nanotubes

We have obtained nanotubes of $ZnCr_2O_4$ by the reaction of Zn nanowire with CrO_2Cl_2. A low magnification FESEM image of the $ZnCr_2O_4$ nanotubes is shown in Figure 6a. The nanotubes replicate the zigzag morphology of the starting Zn nanowires. The nanowires have lengths of several micrometers while the diameter varies between 150 and 500 nm. Open ends of the nanotubes are clearly seen in the FESEM image in Figure 6a. The TEM image of $ZnCr_2O_4$ nanotube in Figure 6b reveals the porous nature of nanotubes. The nanotubes have a granular wall, with a thickness of 20-30 nm. The SAED pattern shows rings, due to the polycrystalline nature of the $ZnCr_2O_4$ nanotubes. The XRD pattern of the nanotubes is characteristic of the cubic structure $ZnCr_2O_4$ (JCPDF card: No. 22-1107, a = 8.32 Å).

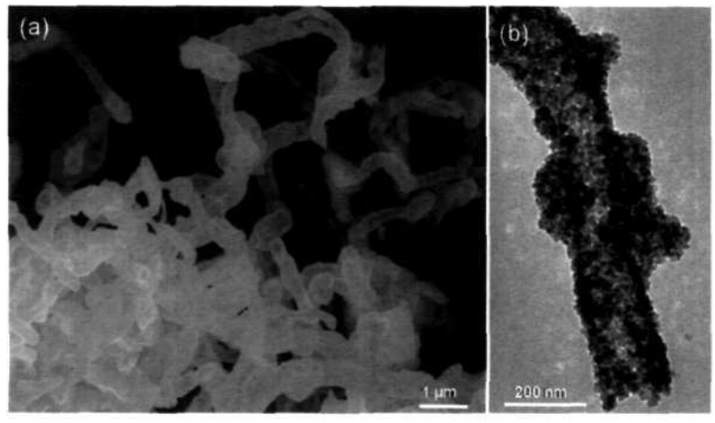

Figure 6. (a) FESEM image of $ZnCr_2O_4$ nanotubes, (b) TEM image of a $ZnCr_2O_4$ nanotube

Co_3O_4 nanotubes

Figure 7a shows a FESEM image of Co nanowires with a necklaces-like structure obtained by the nebulized spray pyrolysis of a methanolic solution of Co acetate. The nanowires have a narrow diameter distribution (20-25 nm range) with lengths of several micrometers. The TEM image in Figure 7b reveals that the nanowires are formed by head to tail fusion of linearly arranged spindle-shaped nanoparticles. A TEM image of a Co_3O_4 nanotube obtained by the thermal oxidation of Co nanowires at 500 °C in air is shown in Figure 7c. The outer diameter of the nanotube is around 40 nm, with a wall thickness of 10 nm. The inner diameter of the nanotube is similar to the diameter of starting Co nanowires indicating that the nanotube is formed by the dominant outer

diffusion of cobalt atoms through the initially formed oxide layer on the surface of nanowires. As the starting nanowires have necklace-like

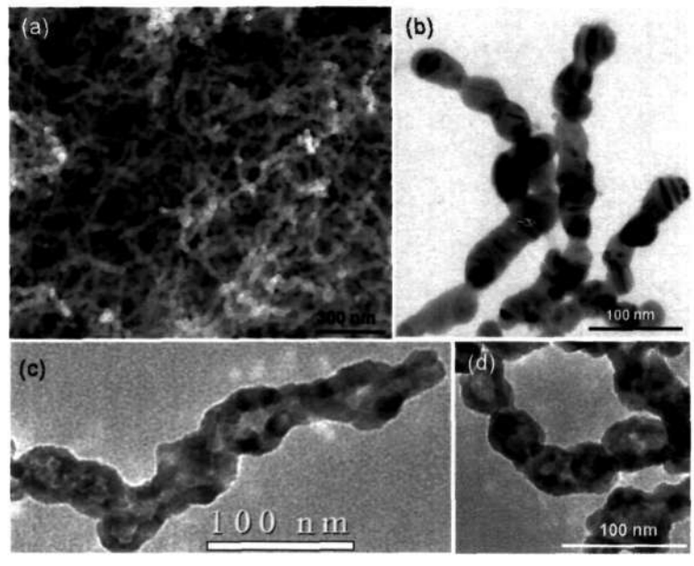

Figure 7. (a) FESEM image and (b) TEM image of Co nanowires, (c) TEM image of a Co_3O_4 nanotube, (d) TEM image of the intermediate stage of a Co_3O_4 nanotube formation

morphology, the walls of the product nanotubes are not parallel and there are some humps at the fusion points. The intermediate stage of the Co_3O_4 nanotubes formation was examined by transmission electron microscopy. The TEM image in Figure 7d reveals that the Kirkendall holes localized inside the interconnected nanoparticles during intermediate stage of oxidation. When heated at higher temperature the localized holes get interconnected to form the continuous tubular structure.

SiO_2 nanotubes

In Figure 8a, we shows a STEM image of Si nanowires obtained by heating an intimate mixture of silicon powder and activated charcoal in a nitrogen environment. The nanowires have diameters ranging from 100 to 400 nm and lengths of several tens micrometers. The XRD pattern of the nanowires shown in Figure 8c matches with that of cubic silicon (JCPDF card: No. 03-0544, a = 5.42 Å). Si nanowires were heated up to 1325 °C to obtain nanotubes of SiO_2 shown in the STEM image in Figure 8b. The diameter of the nanotubes is around 700 nm with wall thickness of around 100 nm. Figure 8c shows the XRD pattern of the

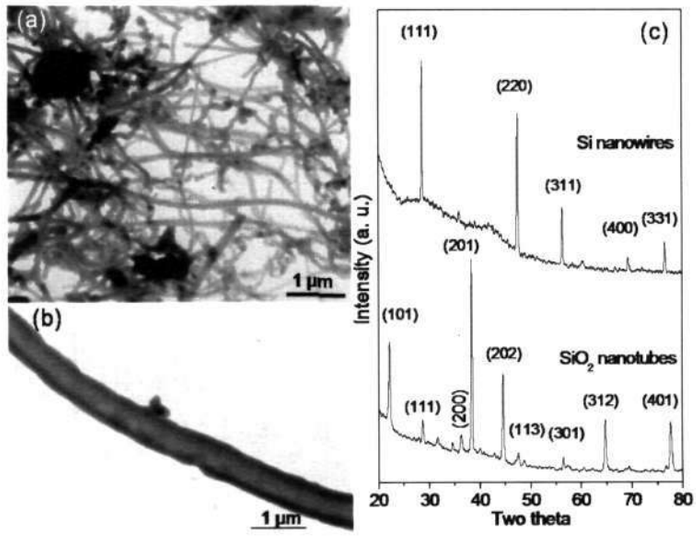

Figure 8. STEM image of (a) Si nanowires and (b) SiO_2 nanotube, (c) XRD patterns of Si nanowires and SiO_2 nanotubes.

nanotubes, the strong intensity of the peaks indicates high crystallinity of the nanotubes. All the peaks could be indexed on the tetragonal SiO_2 structure of cristobalite with the lattice parameters, a = 4.9 Å and c = 6.9 Å (JCPDF card: No. 04-0379). The SiO_2 nanotubes obtained here are unusual in that they are crystalline, unlike most silica nanotubes which are amorphous.

ZnS nanotubes

Reaction of Zn nanowires with sulphur powder yields abundant quantities of ZnS nanotubes. The FESEM image in Figure 9a shows that

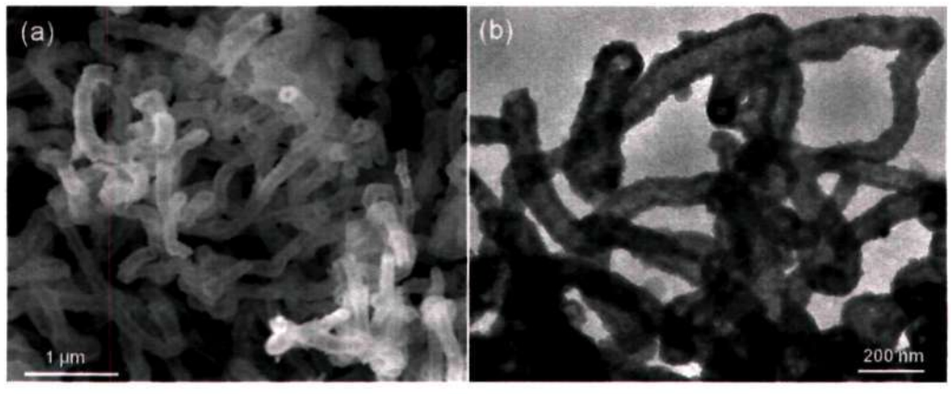

Figure 9. (a) FESEM image and (b) TEM image of ZnS nanotubes.

the ZnS nanotubes have lengths of few microns with zigzag morphology similar to the starting Zn nanowires. A low magnification TEM image of ZnS nanotubes is shown in Figure 9b. The outer diameter of the nanotubes is around 100 nm with wall thickness of 20-25 nm. The XRD pattern of the as prepared nanotubes reveals the formation of phase-

pure ZnS with the cubic structure (JCPDF card: No. 01-0792, a = 5.4 Å).

CdS nanotubes

Cd nanowires prepared by nebulized spray pyrolysis (see the FESEM image in Figure 10a.) had diameters varying from 80 to 400 nm, with lengths of several micrometers. The Cd nanowires have a smooth surface with zigzag morphology. The XRD pattern of the nanowires is characteristic of the hexagonal structure of cadmium (JCPDF card: No. 85-1328, a = 2.97 Å, c = 5.61 Å). Cadmium nanowires were transformed into CdS nanotubes by heating with sulphur powder in an Ar atmosphere at 500 °C for 3h. In Figure 10b we show a FESEM image of the CdS nanotubes. The nanotubes have a smooth surface with diameter in the range of 100 to 500 nm. The length of nanotubes goes up to several microns just as the starting Cd nanowires. A TEM image of an individual CdS nanotube is shown in Figure 10c. The diameter of this nanotube is around 200 nm with a wall thickness of 30-40 nm. The XRD pattern of the CdS nanotubes establishes the hexagonal structure with lattice parameters of a = 4.1 Å and c= 6.7 Å (JCPDF card: No. 01-0783).

The kinetics of the transformation of the Cd nanowires to CdS nanotubes was studied by recording the XRD patterns after different periods of the reaction at 528, 548 and 568 K. These XRD patterns clearly show increase in the intensity of the CdS reflections with time.

The ratios of areas under the (110) reflection of CdS and the (101) reflections of Cd are plotted against time in Figure 10d. The solid lines in Figure 10d show the fits of the experimental data to logarithimic rate

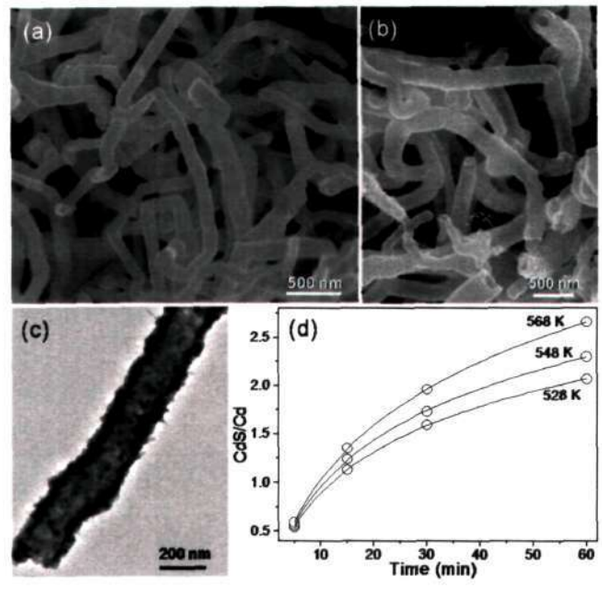

Figure 10. FESEM image of (a) Cd nanowires and (b) CdS nanotubes, (c) TEM image of a CdS nanotube, (d) Plots of the ratios of areas under CdS (110) and Cd (101) reflections against reaction time at different temperatures (open symbols). Solid curves represent the logarithimic rate law fit to the experimental data.

law as given by Equation (1). From the rate constants so obtained, we estimate the activation energy for the conversion to be 8.5 kcal/mol. The activation energy reported for the formation of an anodic film of CdS on a Cd electrode is 10.6 kcal/mol.[27] Formation of CdS nanocrystals starting from Cd-stearate and tributylphosphine sulfide in a paraffin hot matrix involves an activation energy of 51.9 kcal/mol.[28] Thus, the

conversion of Cd nanowires to CdS nanotubes involves a lower activation energy than that for bulk conversions.

CdSe nanotubes

It has been possible to obtain CdSe nanotubes starting from Cd nanowires. In Figure 11a we show a FESEM image of a single CdSe

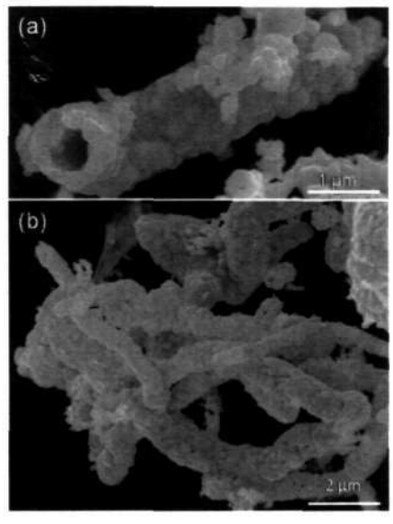

Figure 11. (a) and (b) FESEM image of CdSe nanotubes.

nanotube obtained by heating an intimate mixture Cd nanowires and Se powder. The nanotubes have a diameter of around 800 nm with a wall thickness in the range of 200 to 250 nm. The granular wall of the nanotube is made up of CdSe nanocrystals. A low magnification FESEM image of CdSe nanotubes is shown in Figure 11b. The XRD pattern of the nanotubes is showed to have the cubic structure. (JCPDF card: No. 03-0544, a = 5.42 Å).

4.5 Conclusions

We have investigated the structures as well as the formation kinetics of 1D hollow nanostructure of oxides and other materials formed by the transformation of elemental nanowires through Kirkendall effect. A detailed study of the formation of ZnO nanotubes starting from Zn nanowires has been carried out by employing X-ray diffraction and electron microscopy. The transformation requires only a small activation energy of 12.2 kcal/mol. Nanotubes of $ZnCr_2O_4$ are obtained by the reaction of Zn nanowires with CrO_2Cl_2 in oxygen. It has been possible to obtaine nanotubes of SiO_2, Co_3O_4, ZnS, CdS and CdSe by the reaction of the corresponding elemental nanowires with oxygen or the chalcogen. In the case of SiO_2, the nanotubes are crystalline with the cristobalite structure. The activation energy of formation of CdS nanotubes is also small. The present study demonstrates how Kirkendall effect can be exploited as a novel means of producing nanotubes of a variety of inorganic materials. Furthermore, the study throws light on the mechanism of the Kirkendall effect in forming hollow nanotubes from nanowires.

References

1. A. D. Smigelskas and E. O. Kirkendall, *Trans. AIME,* **171**, *130*, 1947.

2. H. J. Fan, U. Gosele and M. Zacharias, *small,* **3**, *1660*, 2007.

3. E. O. Kirkendall, *Trans. AIME,* **147**, *104*, 1942.

4. D. L. Anton and A. G. Giamei, *Mater. Sci. Eng.,* **76**, *173*, 1985.

5. D. Tomus, K. Tsuchiya, M. Inuzuka, M. Sasaki, D. Imai, T. Ohmori and M. Umemoto, *Scr. Mater.,* **48**, *489*, 2003.

6. J. D. Kelin, G. Warshaw, N. Duziak, S. F. Cogan and R. M. Rose, *IEEE Trans. Magn.,* **17**, *380*, 1981.

7. C. N. R. Rao, and A. Govindaraj, *Nanotubes and nanowires;* RSC publishing: Cambridge, **2005.**

8. C. N. R. Rao, S. R. C. Vivekchand, K. Biswas and A. Govindaraj, *Dalton Trans.,* **34,** *3728*, 2007.

9. Y. Yin, R. M. Rioux, C. K. Erdonmez, S. Hughes, G. A. Somorjai and A. P. Alivisatos, *Science,* **304,** *711*, 2004.

10. C. H. B. Ng, H. Tan and W. Y. Fan, *Langmuir,* **22**, *9712,* 2006.

11. U. K. Gautam, Y. Bando, J. Zhan, P. M. F. J. Costa, X. Fang and D. Golberg, *Adv. Mater.,* **20**, *810,* 2008.

12. H. J. Fan, M. Knez, R. Scholz, K. Nielsch, E. Pippel, D. Hesse, M. Zacharias and U. Gosele *Nat. Mater.,* **5**, *627*, 2006.

13. X. Chen, Z. Zhang, Z. Qiu, C. Shi and X. Li, *J. Colloid Interface Sci.,* **308**, *271*, 2007.

14. S. R. C. Vivekchand, G. Gundiah, A. Govindaraj and C. N. R. Rao, *Adv. Mater.*, **16**, *1842*, 2004.

15. G. Gundiah, F. L. Deepak, A. Govindaraj and C. N. R. Rao, *Chem. Phys. Lett.*, **381**, *579*, 2003.

16. D. Kim, J. Park, K. An, N. K. Yang, J. G. Park and T. Hyeon, *J. Am. Chem. Soc.*, **129**, *5812*, 2007.

17. V. O. Nwoko and H. H. Uhlig, *J. Electrochem. Soc.*, **112**, *1181*, 1965.

18. W. H. J. Vernon, E. A. Calnan, C. J. B. Clews and T. Nurse, *J. Proc. R. London A*, **216**, *375*, 1953.

19. R. A. Konetzki and Y. A. Chang, *J. Mater. Res.*, **4**, *1421*, 1989.

20. N. F. Mott, *Trans. Faraday Soc.*, **43,** *429*, 1947.

21. A. T. J. Formhold, *J. Phys. Chem. Solids*, **24**, *1081*, 1963.

22. D. J. Young and M. J. Dignam, *Oxid. Met.*, **5**, *241*, 1972.

23. B. L. Maschhoff and N. R. Armstrong, *Langmuir*, **7**, *693*, 1991.

24. N. Cobrera and N. F. Mott, *Rep. Prog. Phys.*, **12,** *163*, 1949.

25. W. J. Moore and J. K. Lee, *Trans. Faraday Soc.*, **45**, *501*, 1951.

26. W. J. *J.* Moore, *Chem. Phys.*, **20**, *764*, 1952.

27. L-S. R. Yeh, P. G. Hudson and A. Damjanovic, *J. Appl. Electrochem.*, **12**, *153*, 1982.

28. G. G. Yordanov, E. Adachi and C. D. Dushkin, *Colloids Surf. A.*, **289**, *118*, 2006.